nature chemistry

Article

https://doi.org/10.1038/s41557-022-01073-1

Insights into the ribosome function from the structures of non-arrested ribosomenascent chain complexes

Received: 13 January 2022

Accepted: 23 September 2022

Published online: 31 October 2022



Check for updates

Egor A. Syroegin ® ¹, Elena V. Aleksandrova ¹ and Yury S. Polikanov ® ^{1,2,3} ⊠

During protein synthesis, the growing polypeptide threads through the ribosomal exit tunnel and modulates ribosomal activity by itself or by sensing various small molecules, such as metabolites or antibiotics, appearing in the tunnel. While arrested ribosome-nascent chain complexes (RNCCs) have been extensively studied structurally, the lack of a simple procedure for the large-scale preparation of peptidyl-tRNAs, intermediates in polypeptide synthesis that carry the growing chain, means that little attention has been given to RNCCs representing functionally active states of the ribosome. Here we report the facile synthesis of stably linked peptidyl-tRNAs through a chemoenzymatic approach based on native chemical ligation and use them to determine several structures of RNCCs in the functional pre-attack state of the peptidyl transferase centre. These structures reveal that C-terminal parts of the growing peptides adopt the same uniform \beta-strand conformation stabilized by an intricate network of hydrogen bonds with the universally conserved 23S rRNA nucleotides, and explain how the ribosome synthesizes growing peptides containing various sequences with comparable efficiencies.

Protein biosynthesis, also known as translation, is a key step in the gene expression pathway and is catalysed by the ribosome—one of the most conserved and sophisticated molecular machines of the cell. The ribosome provides a platform for binding the messenger RNA (mRNA) and transfer RNAs (tRNAs). tRNAs serve as adaptor molecules and have two functional ends, one carrying the amino acid and the other end containing the anticodon that recognizes the mRNA codon. tRNAs bind to the ribosome in three places: A (aminoacyl), P (peptidyl) and E (exit) sites. The A site binds the incoming aminoacyl-tRNA (aa-tRNA), the P site retains the peptidyl-tRNA carrying the nascent polypeptide chain, and the E site binds deacylated tRNA before it dissociates from the ribosome. The ribosome is composed of two unequal subunits, small and large (30S and 50S in bacteria), which join together to form functional 70S ribosomes. The small subunit decodes genetic information delivered by mRNA, whereas the large subunit covalently links amino acids into a nascent protein, which is then threaded through the nascent peptide exit tunnel (NPET) that spans the body of the large subunit.

Although NPET was initially thought to be a passive conduit for the growing polypeptide chain, it became clear in recent years that it plays an active role in co-translational protein folding and in the regulation of protein synthesis². For example, some of the most widely used classes of antibiotics, such as macrolides, bind in the NPET of the bacterial ribosome and interfere with the progression of certain growing polypeptides through this tunnel $^{3-5}$. There are also many examples of small molecules and/or metabolites that modulate the rate of translation by binding in the NPET^{2,6}. The binding of an antibiotic or a small-molecule modulator to the NPET and the presence of a nascent peptide with a particular sequence results in a slowdown or even a complete arrest of such ribosome-nascent chain complexes (RNCCs) on the mRNA. This happens because the growing peptide adopts a particular conformation inside the NPET and establishes direct contacts with the walls

Department of Biological Sciences, University of Illinois at Chicago, Chicago, IL, USA. Department of Pharmaceutical Sciences, University of Illinois at Chicago, Chicago, IL, USA. 3Center for Biomolecular Sciences, University of Illinois at Chicago, Chicago, IL, USA. e-mail: yuryp@uic.edu

of the tunnel and a small molecule present there at the same time². Moreover, the synthesis of some nascent chain sequences is intrinsically problematic for the ribosome, with polyproline stretches being the most striking example⁷.

Although molecular mechanisms underlying nascent chain-mediated ribosome stalling have attracted increasing attention in recent years, such events are rare and can occur with relatively few peptide sequences. In fact, evolution has built ribosomes to be able to synthesize most of the cellular proteins without the need for auxiliary factors. Furthermore, the ribosome remains an effective catalyst despite the existing chemical diversity of its multiple amino acid substrates and the possible heterogeneity of growing peptide chain conformations in the NPET. Structural studies of arrested RNCCs can explain why ribosomes become inactive while trying to synthesize particularly problematic amino acid sequences⁸⁻¹³. However, the complementary guestion—'what makes the ribosome a versatile catalyst capable of acting with comparable efficiency upon 20 different aa-tRNA substrates and many possible nascent chain folds within the tunnel?'-has always remained beyond the scope of such studies but could be tackled by the structural analysis of non-arrested RNCCs or their mimics, which represent a functionally active state of the ribosome.

In nearly all structural and biochemical studies of arrested RNCCs⁸⁻ 18, peptidyl-tRNAs were prepared *in cis* by exploiting the natural peptidyl transferase activity of the ribosome to generate peptides attached to tRNAs in the P site. While certainly producing close-to-natural ribosome complexes, this approach allows preparation of homogeneous samples of only the peptide-arrested RNCCs, which represent an inactive state of the peptidyl transferase centre (PTC) by definition. The inability to perform pairwise comparisons of structures of arrested versus non-arrested RNCCs (for example, with versus without antibiotic or a small molecule; wild-type stalling motifs versus mutants) hampers our profound understanding of the underlying ribosome stalling mechanisms. Capturing non-arrested nascent peptides in the pre-peptidyl transfer state remains challenging and requires either a kinetic control¹⁹ or use of hydrolysis-resistant aa-tRNAs²⁰ to prevent transpeptidation reaction. To date, the only reported structures of the ribosome in the pre-peptidyl transfer state of the PTC contain a minimal possible P-site substrate, fMet-tRNA, which allows visualizing only a single first amino acid of the nascent peptide but not a longer polypeptide chain within the ribosome tunnel^{19,20}. There are no available structures of the ribosome functional complexes containing both aa-tRNA in the A site and peptidyl-tRNA in the P site in the pre-peptidyl transfer state, which is in part due to the lack of a simple and reliable procedure for the large-scale preparation of peptidyl-tRNAs.

Alternatively, peptidyl-tRNAs can be prepared using a combination of synthetic and biochemical techniques and subsequently added in trans to ribosomes to form the desired RNCCs²¹. This approach is based on the in vitro translation-independent preparation of the peptidyl-tRNAs, allows incorporation of unnatural amino acids, and of fluorescent or stable isotope labels for FRET and NMR studies, and, in general, provides more flexibility and control over what is being charged to the tRNAs. To be more suitable for structural studies, especially for X-ray crystallography or NMR, the peptide moiety of the peptidyl-tRNA must be amide-linked to the CCA end of the tRNA to prevent spontaneous hydrolysis and deacylation during the time course of $the\, experiments^{18,20}.\, Although\, such\, hydrolysis\text{-}resistant\, tRNAs\, do\, not\, although\, such\, hydrolysis\text{-}resistant tRNAs\, do\, not\, although\, such\, hydrolysis\text{-}resistant\, such\, hydrolysis - although\, such\, hydrolysis$ represent natural substrates per se, they have not only been shown to be structurally indistinguishable from native tRNA substrates 19 but are also active in transpeptidation when placed in the A site and combined with native aa-tRNA in the P site^{20,22}, and therefore represent a reasonable approximation of the reactive state, one that is accurate enough to allow mechanistic hypotheses to be formulated.

Here we report a chemoenzymatic approach based on a native chemical ligation (NCL) reaction for the facile synthesis of both stable amide-linked as well as labile ester-linked peptidyl-tRNAs carrying

peptide chains of the desired sequences that can be used in a wide range of structural and/or biochemical studies of both arrested and non-arrested RNCCs. We also report several structures of non-arrested RNCCs in the pre-attack state of the PTC. These structures reveal a previously unknown role of the ribosome in stabilizing the growing polypeptide chain within the PTC and suggest an extended entropic trap model that mechanistically rationalizes how ribosome acts with comparable efficiency upon a multitude of possible nascent chain sequences. Moreover, unlike previous views that ribosome generates the α -helical conformation at the C-terminus of the nascent peptide, a detailed analysis of our structures suggests that, regardless of the sequence, the C-terminal non-proline residues of the nascent peptide emerge in the uniform zigzag β -strand conformation that is stabilized by the intricate network of hydrogen bonds (H-bonds) provided by the universally conserved 23S rRNA nucleotides.

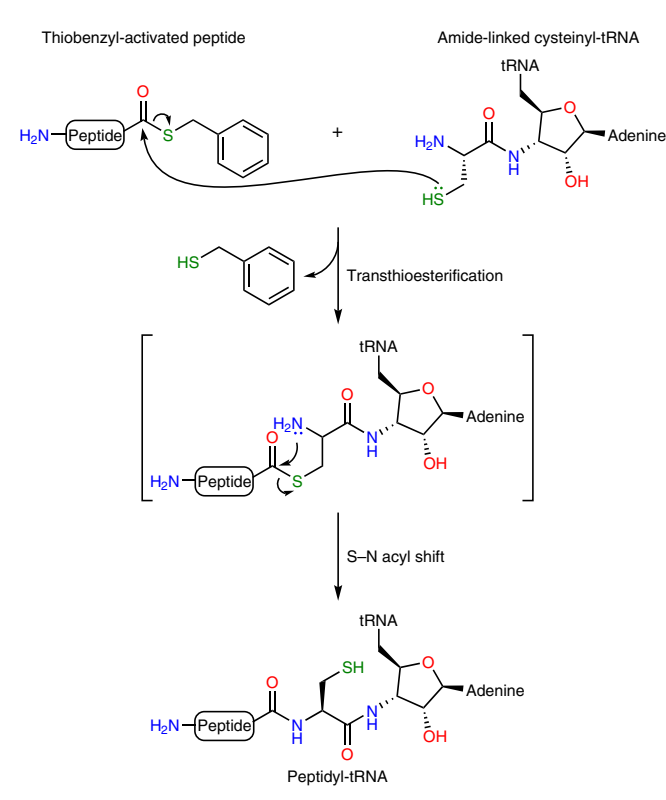
Results

NCL-based synthesis of non-hydrolysable peptidyl-tRNAs

The synthesis of non-hydrolysable peptidyl-tRNAs is challenging because there are no enzymes that can directly attach desired peptides to a deacylated tRNA. Only one method for the preparation of non-hydrolysable peptidyl-tRNA has so far been reported, which involves customized solid-phase synthesis of the precursors²³ and is therefore challenging to perform in a standard molecular biology laboratory, precluding the wide use of this approach by researchers. Moreover, such an approach requires laborious tRNA engineering with DNA enzymes, and enzymatic ligation steps to include the native tRNA nucleoside modifications²³. Thus, the utility of the *in trans* RNCC reconstitution approach is greatly limited by the lack of a facile and reliable procedure for the large-scale synthesis of stable peptidyl-tRNAs.

To bridge this gap, we have established a simple method for the semi-synthesis of non-hydrolysable peptidyl-tRNAs using the NCL reaction, which was originally developed for linking unprotected peptide fragments with each other under mild reaction conditions²⁴. NCL is based on a reaction between an activated C-terminal thioester of the first peptide fragment and the N-terminal cysteine residue of the second peptide fragment, resulting in the formation of a native peptide bond between the two fragments. In the method that we report here, we used aminoacyl-tRNA charged with cysteine as the C-terminal reactant, while as the N-terminal reactant, we used a peptide with the desired sequence and activated with the thiobenzyl (TBZ) group, which is now available commercially as a C-terminal modification through the majority of vendors providing peptide synthesis (Fig. 1). Previously, the Micura group utilized NCL for the synthesis of short peptidyl-tRNA mimics comprising only the CCA-ends²⁵. However, those early procedures relied heavily on laborious and advanced organic synthesis methods to prepare the non-standard solid supports, essentially making them inaccessible to a general molecular biology laboratory. Moreover, flexizymes have been used in the past to charge 3'-NH₂-tailed tRNAs with a single amino acid²⁶, which in principle should work for peptides as well. However, no successful applications of the flexizyme-based methodology for charging amino-tailed tRNAs with a peptide appear to have been reported. The advantage of our chemoenzymatic approach is that it utilizes only commonly available equipment, affordable chemicals and universally available commercial peptide synthesis services, and can therefore be employed by virtually any laboratory.

The overall procedure comprises three steps (Fig. 2a): (1) tRNA-tailing to replace the 3'-terminal regular adenosine-3'-OH of the CCA-end with its amino-substituted adenosine-3'-NH₂ analogue^{27,28}; (2) enzymatic charging of the tailed 3'-NH₂-tRNA with cysteine by the aminoacyl-tRNA-synthetase^{27,28}; and (3) native chemical ligation of the TBZ-activated peptide with cysteinyl-tRNA to yield the final product (Fig. 1). It would have been logical to use cysteine-specific tRNA^{Cys} to prepare the non-hydrolysable cysteinyl-NH-tRNA needed for the NCL. However, in our pilot experiments, we have found that



 $\label{lem:problem:p$

methionine-specific aminoacyl-tRNA-synthetase (MetRS) can efficiently mischarge the tailed initiator 3'-NH₂-tRNA_i^{Met} with cysteine resulting in >90% yields (Fig. 2b, lane 2 versus 3), which probably happens due to the compromised editing activity of this ARSase as a result of its inability to hydrolyse non-hydrolysable aa-tRNA²⁹. The main advantage of using the initiator tRNA_i^{Met} instead of tRNA^{Cys} as the P-site substrate for the subsequent ribosome structural studies stems from its high affinity for the ribosomal P-site, ensuring the proper binding of the tRNA body to the ribosome. Moreover, unlike tRNA^{Cys}, the procedure for large-scale preparation of tRNA_i^{Met} is well established^{20,27,28,30}.

For the first NCL trials, we have selected several model peptides of different lengths and sequences that would also be interesting to study beyond the scope of this work (Extended Data Fig. 1a). We should note that some of the peptide sequences in our list represent known ribosome stalling motifs, which, however, cause translation arrest only in the presence of a particular drug (such as PTC-targeting antibiotic chloramphenicol in the case of hns, or macrolide antibiotics in the case of ermDL gene products), but otherwise are translated normally and should be considered as non-arresting peptides in the absence of the corresponding drug molecules, thereby representing merely model cases for our structural studies. Using the TBZ-activated peptides (purchased from NovoPro Biosciences) and the Cys-NH-tRNA_i^{Met} as the N- and C-terminal fragments for the NCL reaction, respectively, we show that most of the selected peptides can be efficiently ligated to the Cys-NH-tRNA_i^{Met} with yields exceeding 50% (Fig. 2b, lane 3 versus 4, and Extended Data Fig. 1b). We used treatment with proteinase K, which hydrolyses the amide bond between the peptide moiety and the tRNA (ref. 31), to confirm the presence of the peptidyl moiety attached to the tRNA_i^{Met} (Fig. 2c, odd versus even lanes). Even by using the previously reported conditions for peptide ligation²⁴, the efficiency of NCL was already sufficiently high (>50%). Nevertheless, by searching for optimal reactant concentrations, and types and combinations of catalysts and denaturing agents used for the NCL (Methods), we have achieved >70% reaction efficiency for several peptides. Thus, by using the NCL approach, we have synthesized a set of non-hydrolysable full-length peptidyl-tRNAs carrying various peptide sequences at their CCA-ends, which were then purified by reverse-phase chromatography and used directly for ribosome complex formation and structure determination.

We have also checked whether cysteine-specific tRNA^{Cys} in combination with the cysteinyl-tRNA-synthetase could be used for our NCL-based technique. Using optimized conditions for the aminoacylation reaction (Methods), we have prepared non-hydrolysable pentapeptidyl-tRNA with the formyl-Met-Ser-Glu-Ala-Cys peptide moiety, designated as fMSEAC-NH-tRNA^{Cys} (Extended Data Fig. 2a). Moreover, by skipping the tRNA-tailing step, we were able to prepare regular ester-linked fMSEAC-O-tRNA^{Cys} (Extended Data Fig. 2b), suggesting that this method is not limited to the preparation of only non-hydrolysable amide-linked peptidyl-tRNAs.

In trans addition of the peptidyl-tRNAs results in the formation of functionally relevant pre-peptidyl transfer ribosome complexes

Next, to check whether the obtained full-length peptidyl-tRNAs can be used for structural studies of the non-arrested RNCCs, we prepared a complex of *Thermus thermophilus* 70S ribosome programmed with 24-nt-long mRNA and also containing cognate full-length P-site fMSEAC-NH-tRNA_i^{Met} and A-site Phe-NH-tRNA^{Phe}, crystallized it, and determined its structure at 2.4 Å resolution (Fig. 3a,b). The observed high-quality electron density maps for both A- and P-site tRNA substrates (Fig. 3c) allowed unambiguous modelling of four out of the five amino acid residues in the fMSEAC-peptide attached to the CCA-end of the P-site tRNA (Fig. 3d–f). We observed no electron density for the N-terminal formyl-methionine residue of the fMSEAC-peptide, which is probably due to the lack of coordination with the surrounding nucleotides of the 23S rRNA, resulting in its high flexibility.

We then aligned our structure containing fMSEAC-peptidyl-tRNA with the previously published structures of the 70S ribosome in the pre-attack state containing either the non-hydrolysable amide-linked (Extended Data Fig. 3a)^{20,28} or native ester-linked full-length aa-tRNAs in the A and P sites (Extended Data Fig. 3b)¹⁹. We found no major structural differences in the positions of the CCA moieties (Extended Data Fig. 3a,b) or in most of the key 23S rRNA nucleotides around the PTC (Extended Data Fig. 3c. d), suggesting that this structure also represents a functionally relevant pre-attack state of the peptidyl-tRNA (Fig. 3e), even though the peptidyl-tRNA was added to the ribosome in trans. In particular, the orientation of the attacking α-amino group of the aa-tRNA relative to the carbonyl carbon of the P-site substrate is nearly identical between the structures harbouring amide-linked versus native ester-linked full-length aminoacyl- and peptidyl-tRNAs in the A and P sites, respectively (Fig. 3e and Extended Data Fig. 3a,b)²⁰, indicating that stable amide-linked aminoacyl- and peptidyl-tRNAs are adequate mimics of their native labile ester-linked counterparts. Our structural comparison reveals somewhat different conformations of highly flexible nucleotides A2062 and A2602 of the 23S rRNA (Extended Data Fig. 3d), which is probably due to their uncertain positions in the previous Escherichia coli ribosome structure¹⁹ resulting from lower resolution and lack of cryo-electron microscopy (cryo-EM) density.

It is important to emphasize that using stable aminoacyl-/peptidyl-tRNAs allows trapping of the ribosome in the pre-peptidyl-transfer state because PTC is unable to cleave the amide bond connecting peptide to the tRNA so that peptidyl-tRNA is unable to donate its fMSEAC moiety to form a peptide bond with the A-site amino acid residue. This methodology of RNCC preparation is different in principle from previous approaches used to produce stalled RNCCs, in which translation arrest happens not because substrates are chemically unreactive but because either the key nucleotides of the catalytic site are perturbed 9,32, or incoming aa-tRNA cannot

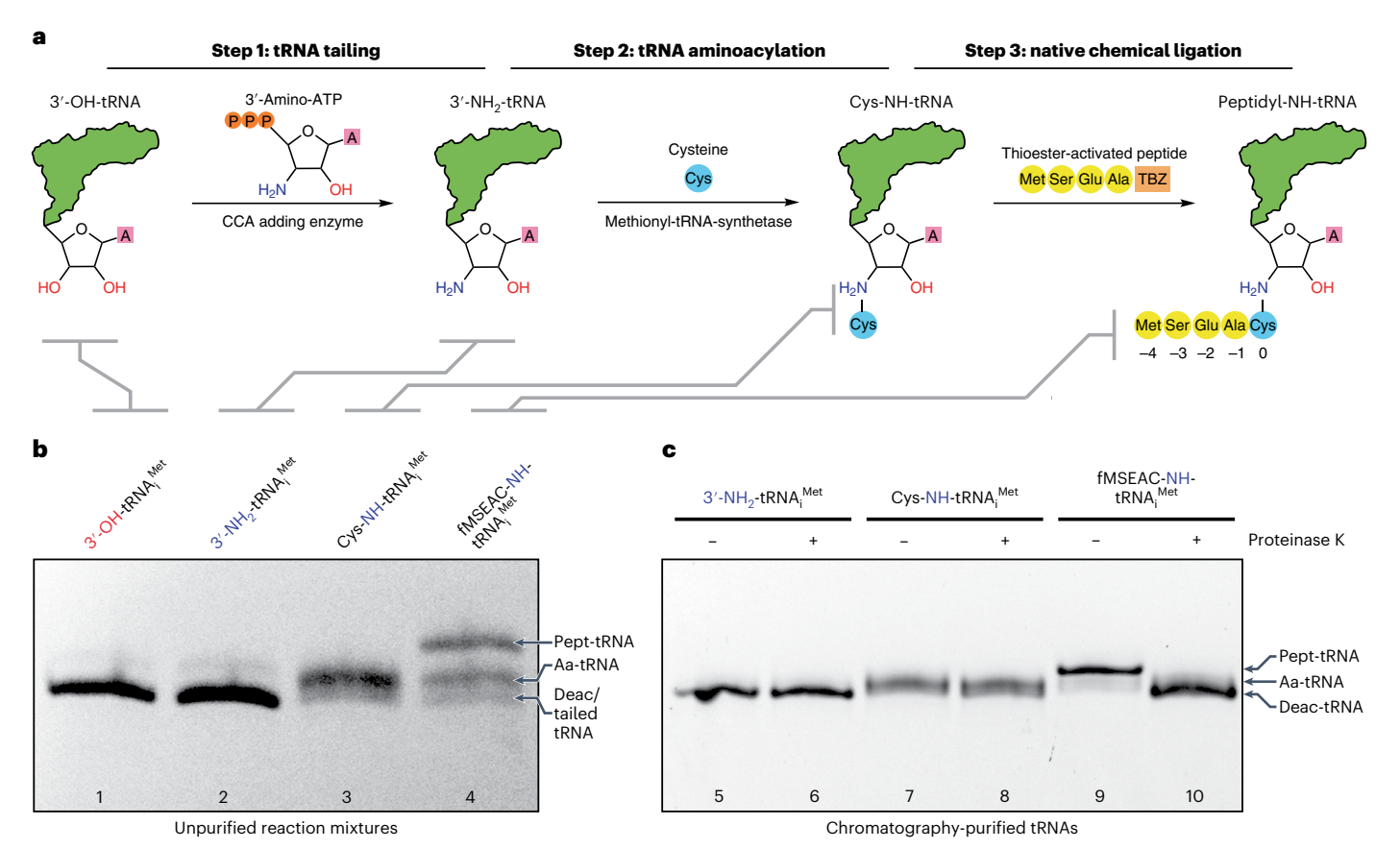


Fig. 2 | **Synthesis of full-length non-hydrolysable peptidyl-tRNAs by NCL. a**, Steps in the preparation of non-hydrolysable peptidyl-tRNAs. The first tRNA-tailing step was performed via exchange of the natural 3′-OH-AMP moiety of tRNA with the 3′-NH $_2$ -AMP by using the CCA-adding enzyme 27 . The body of the tRNA is shown in green. **b, c**, Electrophoretic separation of native *E. coli* tRNA $_1$ ^{Met} (lane 1) after tRNA-tailing reaction (lanes 2, 5, 6); MetRS-driven aminoacylation with cysteine (lanes 3, 7, 8); and native chemical ligation reaction (lanes 4, 9, 10). Unpurified samples shown in **b** were treated (+) or not treated (–) with

proteinase K and chromatography-purified before running on the gel shown in **c**. Electrophoresis of the tRNA samples was performed in 20-cm-long 8% polyacrylamide gel with 7 M urea and stained with ethidium bromide. Note that the slower mobility of tRNA after the NCL (lane 3 versus 4) and its sensitivity to the proteinase K treatment (lane 9 versus 10) confirms the presence of the peptidyl moiety attached to the tRNA $_{\rm i}^{\rm Met}$. Pept, peptidyl; Aa, aminoacylated; Deac, deacylated.

efficiently accommodate into the A site¹¹, or the C-terminal part of the peptidyl-tRNA adopts a non-productive conformation⁸. From this perspective, despite featuring unreactive substrate analogues in the PTC, our ribosome complexes represent non-arrested RNCCs containing full-length aminoacyl- and peptidyl-tRNAs, also providing the highest-resolution view of the PTC in the functional pre-attack state immediately before peptide bond formation.

An extensive H-bond network tightly coordinates growing peptide chains

The structure of fMSEAC-peptidyl-tRNA in the ribosomal NPET reveals tight coordination of the PTC-proximal part of the nascent polypeptide by the elements of the ribosome. In particular, we observe four H-bonds between the nucleotides of the 23S rRNA and the three C-terminal amino acid residues of the nascent peptide, and an additional intramolecular H-bond between the C-terminal residues of the nascent peptide. The carbonyl and amide groups of the penultimate (–1) residue in the fMSEAC-peptide (Ala4) are coordinated by the universally conserved 23S rRNA nucleotides G2061 and A2062, respectively (Figs. 3f and 4a,b, HB-1 and HB-2). At the same time, the N3 and O4 atoms of the nucleotide U2506 form two additional H-bonds with the carbonyl and amide groups of the (–2) residue of the fMSEAC-peptide (Glu3), respectively (Figs. 3f and 4a,b, HB-3 and HB-4). Another interesting intramolecular H-bond is formed between the amide group of the ultimate residue (Cys) of the peptide and the carbonyl group of the (–2) amino acid

(Glu3) (Figs. 3e and 4a, HB-5). Consistent with previous structural studies, the carbonyl group of the last amino acid residue of the peptide is coordinated by the nucleotide A2602 of the 23S rRNA via a water molecule (referred to as W2 in ref. 20) that was previously proposed to play a key role in stabilizing the tetrahedral oxyanion intermediate of the transition state (Extended Data Fig. 4) 20,33 . We also observe the two other tightly coordinated water molecules in the PTC (referred to as W1 and W3 in ref. 20) that were suggested to take part in the formation of an intricate network of H-bonds, the proton wire, needed for efficient deprotonation of the attacking α -amine during the initial rate-limiting step and the subsequent breakdown of the transition-state intermediate (Extended Data Fig. 4) 20 .

Ribosome catalyses peptide bond formation by stabilizing the transition-state intermediate and ensuring that the nucleophilic attack by the α -amino group of the aa-tRNA is coordinated with its efficient deprotonation during the rate-limiting step of the reaction 20,34,35 . However, for the reaction to even start, the two reactants must be optimally positioned relative to each other in the PTC 36 . The tight coordination observed here of the C-terminus of the growing peptide inside the NPET can not only ensure the proper fixation of the carbonyl group of the peptidyl-tRNA in the PTC required for efficient attack by the nucleophile to occur, but can also prevent premature peptidyl-tRNA drop-off while the peptide remains relatively short 37,38 . Although the contribution of the ribosome to the A- and P-site substrate stabilization was evident from the previous high-resolution structures 20,28,33 , it was

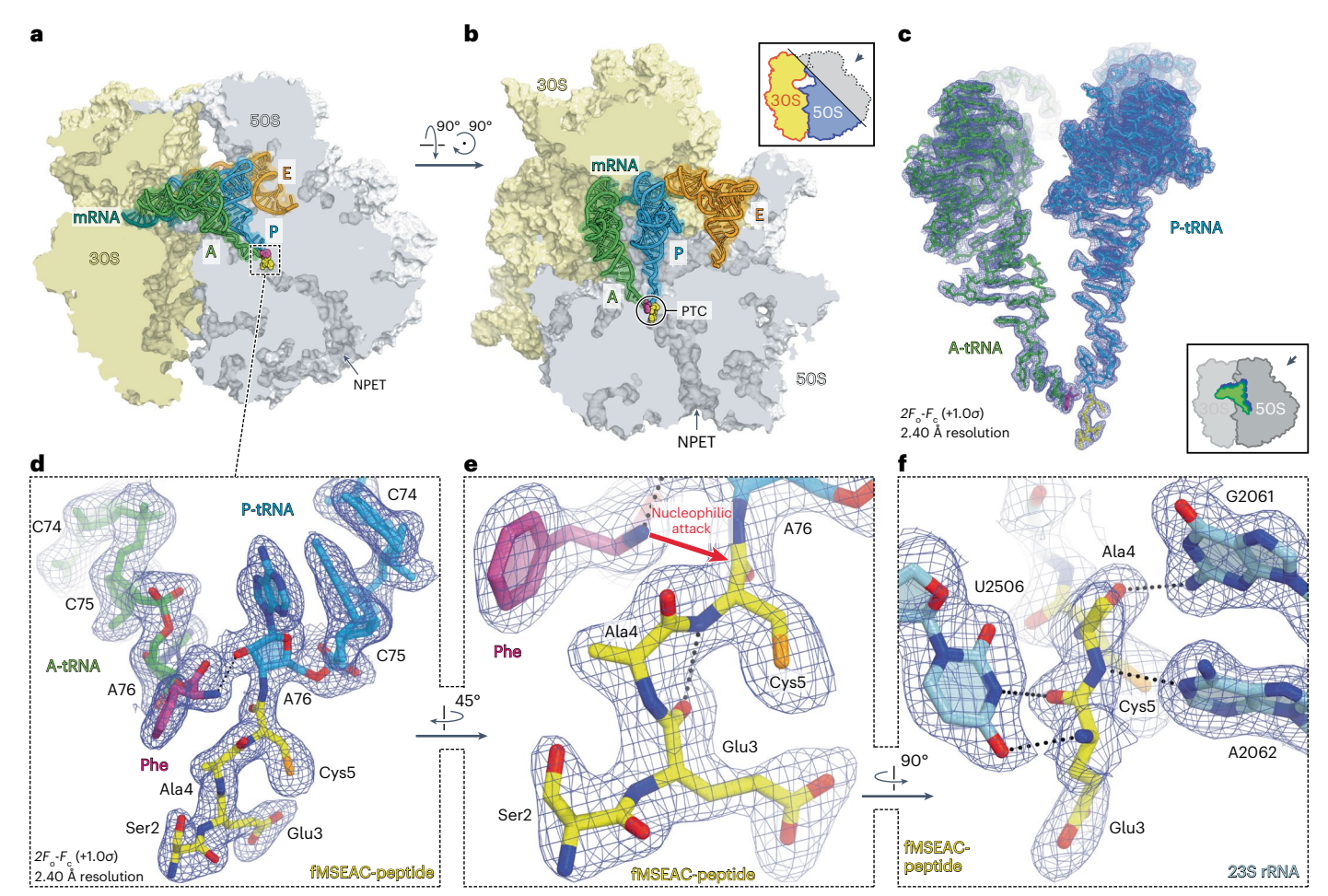


Fig. 3 | **Structure of the 70S ribosome in complex with** | **fMSEAC-peptidyl-tRNA. a,b**, Structure of the *T. thermophilus* 70S ribosome containing full-length aa-tRNA (Phe-NH-tRNA Phe) and peptidyl-tRNA (fMSEAC-NH-tRNA, Met) in the A and P sites, respectively, viewed from two different perspectives (panels $\bf a$ and $\bf b$). The 30S subunit is shown in light yellow, the 50S subunit is in light blue, the mRNA is in teal, and the A-, P- and E-site tRNAs are green, blue and orange, respectively. The phenylalanyl and peptidyl moieties of the A- and P-site tRNAs are magenta and yellow, respectively. The direction of the view in $\bf b$ is indicated by the inset. $\bf c$, High-resolution (2.4 Å) $2F_o-F_c$ electron difference Fourier map (blue mesh) of the ribosome-bound A- and P-site tRNAs. The refined models of tRNAs are displayed in their respective electron density

maps contoured at 1.0σ . The entire bodies of the A- and P-site tRNAs are viewed from the back of the 50S subunit, as indicated by the inset. Ribosome subunits are omitted for clarity. $\mathbf{d}-\mathbf{f}$, Close-up views (from different angles) of the CCA-end of the A-site tRNA carrying a phenylalanyl (magenta) moiety and the CCA-end of the P-site tRNA carrying an fMSEAC-peptidyl (yellow) moiety. Nitrogen atoms, blue; oxygen atoms, red. H-bonds are shown by black dotted lines. Note that the H-bond between the α -amino group and the 2′-OH of the A76 of the P-site tRNA is pivotal for optimal orientation of α -amine for an inline nucleophilic attack onto the carbonyl carbon of the P-site substrate. Interactions of the fMSEAC-peptide with the nucleotides of the 23S rRNA (light blue) are shown in \mathbf{f} .

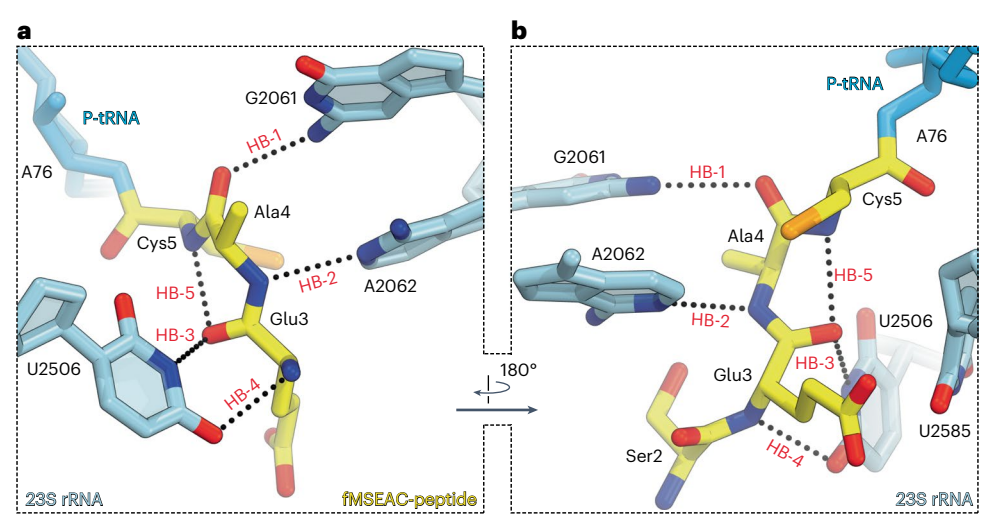
not known that ribosome stabilizes more than just the carbonyl group of the C-terminal residue of the growing peptide. While universally conserved and essential nucleotides A2451, A2602 and C2063 of the 23S rRNA have been suggested to participate in deprotonation of the attacking α -amino group 20 , the individual roles of other important PTC nucleotides remained unclear. The network of H-bonds observed here formed by the universally conserved (G2061, A2062, U2506) and also functionally essential (G2061, U2506) nucleotides of the PTC $^{39-41}$ suggests their primary role in peptidyl-tRNA substrate stabilization. It is also evident from the structure that other nucleobases at positions 2061, 2062 and 2506 would be unable to form the same set of H-bonds, rationalizing their evolutionary conservation.

Interestingly, unlike poorly active U2506 or G2061 mutants, substitutions of A2062 have only modest effects on GFP translation in vitro⁴¹, suggesting dispensability of A2062 for the translation of at least this particular protein (GFP). Furthermore, in vitro translation of the short ErmCL peptide or the ribosomal protein L12 tolerates even the total absence of the nucleobase at this position⁴². However, A2062 is critical for ribosome stalling on the same ErmCL leader sequence (and also

ErmAL) in response to macrolide antibiotics and for natural arrest on SecM 42,43 , pointing to the importance of this nucleotide for cellular functions. Due to its high flexibility, this nucleotide was suggested to be involved in the allosteric regulation of the PTC 43 . These data altogether allow us to hypothesize that, by forming H-bond-2 (Fig. 4) with nascent peptides, nucleotide A2062 performs 'fine-tuning' of the PTC function required either for efficient transpeptidation or efficient translation arrest of particular nascent chain sequences.

Nascent peptides emerge in the uniform $\beta\text{-strand}$ conformation at the PTC

In contrast to many published cryo-EM structures of various RNCCs, most of which represent arrested (and thus inactive) ribosome complexes, in which PTC is unable to catalyse transpeptidation, our structure provides the first snapshot of the PTC in the functional pre-attack state with both A- and P-site substrates bound. Interestingly, Ramachandran plot analysis reveals that the three C-terminal peptide residues of fMSEAC-peptidyl-tRNA appear in a β -strand conformation (Extended Data Fig. 5a).



 $\label{eq:Fig.4} \textbf{Fig. 4} | \textbf{Tight coordination of the PTC-proximal part of the nascent peptide in the NPET. a,b, Close-up views of the interactions between the universally conserved nucleotides G2061, A2062 and U2506 of the 23S rRNA (light blue) and the main chain groups of the ribosome-bound fMSEAC-peptidyl-tRNA (yellow) in the ribosomal exit tunnel. An additional intramolecular H-bond is formed between the residues of the peptide. H-bonds are shown by black dotted lines$

and are annotated as HB-1 to HB-5. Nitrogen atoms, blue; oxygen atoms, red. The directions of the views in panels $\bf a$ and $\bf b$ are opposite. Note that all of these interactions involve only the main-chain atoms of the peptide, suggesting that, in principle, a peptide of any sequence (except for those containing prolines) should be coordinated the same way.

Comparisons of our structure with the available highest-resolution cryo-EM structures of several arrest peptides revealed that the overall trajectories of the C-terminal segments of SpeFL (2.7 Å)¹², ErmDL $(2.9 \text{ Å})^{11}$ and VemP $(2.9 \text{ Å})^{13}$ peptides in the NPET are similar to the path of the fMSEAC-peptide (Extended Data Fig. 6a-c)¹¹⁻¹³. The differences in the paths of the peptides become more prominent as we move further away from the C-terminus. We have also compared this structure of the full-length peptidyl-tRNA to the recent structures of pre-peptidyl transfer complexes featuring short tripeptidyl-tRNA analogues in the P site and ACC-Pmn in the A site (Extended Data Fig. 6d-f)⁴⁴. These peptidyl-tRNA mimics contained only the ACCA tetranucleotide corresponding to the 3' terminus of a full-length tRNA that was attached to one of the three tripeptides via a non-hydrolysable bond to yield ACCA-IAM, ACCA-ITM or ACCA-IFM conjugates. Despite the missing tRNA body, these analogues exhibited not only the same exact placement of all the nucleotides but also highly similar peptide trajectories with nearly identical positions of main-chain and Cβ atoms in comparison to the structure with fMSEAC-peptidyl-tRNA (Extended Data Fig. 6d-f)⁴⁴. Because structures with the short tRNA analogues also represent non-arrested pre-peptidyl transfer ribosome complexes and also contain peptides with various sequences, it is tempting to suppose that any three C-terminal residues (except for prolines) of the growing peptide would always emerge in the same uniform β-strand-like conformation that is strictly enforced by the PTC via multiple H-bonds described above. In principle, there is enough space in the pockets next to the side chains of residues at position -2 (Glu in fMSEAC) or position 0 (Cys in MSEAC) to accommodate any of the proteinogenic amino acids. However, the side chain of the residue at position -1 (Ala in fMSEAC) points towards the confined space of the ribosomal A site, raising the possibility that a large side chain at this position might not be able to fit snugly, resulting in sequence-specific alterations of the peptide path in the NPET and a different secondary structure.

To address this possibility and check whether or not bulky residue in the penultimate position of the nascent peptide can affect its trajectory in the NPET, we synthesized and purified peptidyl-tRNAs carrying formyl-Met-Arg-Cys (fMRC) and formyl-Met-Thr-His-Ser-Met-Arg-Cys (fMTHSMRC) peptides (Extended Data Fig. 1b, lanes 2 and 5) with the largest possible amino acid side chain (Arg) in the penultimate position using our NCL-based approach and determined their structures

in complex with the ribosome. Except for the C-terminal Leu-to-Cys substitution, which does not affect activity⁴⁵, both of these sequences represent short and long versions of the macrolide-dependent arrest peptide ErmDL, respectively^{11,32,45}. Appearance of either of these peptide sequences in the NPET results in translation arrest and ribosome stalling, but only in the presence of a macrolide antibiotic and only if combined with lysyl- or arginyl-tRNA in the A site⁴⁵. Otherwise, these sequences are translated normally and do not cause translation arrest.

Crystals containing *T. thermophilus* 70S ribosome in complex with either the P-site fMRC-NH-tRNA_i Met or fMTHSMRC-NH-tRNA_i and the A-site Phe-NH-tRNA Phe diffracted to 2.5 Å and 2.3 Å resolution, respectively (Table 1). The obtained experimental electron density maps for the corresponding peptidyl-tRNAs allowed unambiguous placement of all of their peptide residues (Fig. 5a-c), including the N-terminal residues for the longer fMTHSMRC-heptapeptide (Fig. 5d.e). Most importantly, both peptides appear to be coordinated by the same exact network of H-bonds (Fig. 5c) as the three C-terminal residues of the fMSEAC-peptide (Fig. 3f). Moreover, the side chains of penultimate arginines in both peptides establish electrostatic interactions with the phosphate of G2505, further anchoring these peptides in the NPET (Extended Data Fig. 7a,b). Surprisingly, but despite being longer than fMSEAC, for which only the four C-terminal residues could be resolved, all residues of the fMTHSMRC-heptapeptide are visible in the electron density map. Most likely, this is due to the prominent π - π stacking interaction of the histidine residue with the nucleobase of A2062, resulting in the overall higher rigidity of the entire ribosome-bound peptide (Extended Data Fig. 7c).

Remarkably, the presence of bulky arginine side chain in the penultimate position of fMRC or fMTHSMRC peptides does not affect their paths in the NPET (Fig. 5f), supporting the hypothesis that, regardless of the sequence, the C-terminal non-proline residues of the nascent peptides emerge in the same uniform zigzag β -strand conformation (Extended Data Fig. 5b,c) that is stabilized by the intricate network of H-bonds provided by the universally conserved nucleotides G2061, A2062 and U2506 of the 23S rRNA. This experimental finding contradicts the previous view that ribosome, by default, generates α -helical conformation at the C-end of the nascent peptide, which was inspired by theoretical calculations 46 . The observed fixation of the PTC-proximal part of the peptide in the NPET is likely to be important

Table 1 | X-ray data collection and refinement statistics

	70S ribosome complex with A-site Phe-NH-tRNA ^{Phe} , and P-site fMSEAC-NH-tRNA _i ^{Met} PDB entry 8CVJ	70S ribosome complex with A-site Phe-NH-tRNA ^{Phe} , and P-site fMRC-NH-tRNA _i ^{Met} PDB entry 8CVK	70S ribosome complex with A-site Phe-NH-tRNA ^{Phe} , and P-site fMTHSMRC-NH-tRNA _i ^{Met} PDB entry 8CVL
Data collection			
Space group	P2 ₁ 2 ₁ 2 ₁	P2 ₁ 2 ₁ 2 ₁	P2 ₁ 2 ₁ 2 ₁
Cell dimensions			
a, b, c (Å)	210.47×451.32×627.74	210.47×451.32×627.74	209.43×447.70×618.27
a, β, γ (deg)	90.0, 90.0, 90.0	90.0, 90.0, 90.0	90.0, 90.0, 90.0
Resolution (Å)	175-2.40 (2.46-2.40) ^a	191-2.50 (2.56-2.50) ^a	187-2.30 (2.36-2.30) ^a
R _{merge}	16.2 (139.5)	18.7 (150.7)	14.6 (141.0)
Ι/σΙ	8.96 (1.00) ^b	7.99 (0.93)°	6.54 (0.83) ^d
Completeness (%)	98.1 (95.5)	99.6 (98.6)	97.5 (94.0)
Redundancy	4.94 (4.80)	5.79 (4.88)	3.44 (3.40)
Refinement			
Resolution (Å)	2.40	2.50	2.30
Number of reflections	2,248,924	2,012,292	2,467,334
R _{work} /R _{free}	24.6/29.5	23.5/28.4	23.7/28.1
Number of atoms			
Protein	91,020	91,008	91,070
Ligand/ion	203,081	203,087	203,042
Water	4,076	4,118	3,983
B factors			
Protein	51.8	51.0	55.9
Ligand/ion	50.0	49.0	53.6
Water	35.5	34.5	40.0
r.m.s. deviations			
Bond lengths (Å)	0.004	0.004	0.004
Bond angles (deg)	0.872	0.851	0.861

Values in parentheses are for the highest-resolution shell. Diffraction data from a single crystal were used to obtain the structure. Diffraction data from a single crystal were used to obtain the structure. Diffraction data from a single crystal were used to obtain the structure. Diffraction data from a single crystal were used to obtain the structure. Diffraction data from a single crystal were used to obtain the structure. Diffraction data from a single crystal were used to obtain the structure. Diffraction data from a single crystal were used to obtain the structure. Diffraction data from a single crystal were used to obtain the structure. Diffraction data from a single crystal were used to obtain the structure. Diffraction data from a single crystal were used to obtain the structure. Diffraction data from a single crystal were used to obtain the structure. Diffraction data from a single crystal were used to obtain the structure. Diffraction data from a single crystal were used to obtain the structure. Diffraction data from a single crystal were used to obtain the structure. Diffraction data from a single crystal were used to obtain the structure. Diffraction data from a single crystal were used to obtain the structure. Diffraction data from a single crystal were used to obtain the structure. Diffraction data from a single crystal were used to obtain the structure. Diffraction data from a single crystal were used to obtain the structure. Diffraction data from a single crystal were used to obtain the structure. Diffraction data from a single crystal were used to obtain the structure. Diffraction data from a single crystal were used to obtain the structure. Diffraction data from a single crystal were used to obtain the structure. Diffraction data from a single crystal were used to obtain the structure. Diffraction data from a single crystal were used to obtain the structure. Diffraction data from a single crystal were used to obtain the structure. Diffraction data from a single crystal were used to obtain the

for the efficient catalytic function of the PTC and/or to prevent possible peptidyl-tRNA drop-off.

Discussion

The main finding of this study is the intricate network of H-bonds that tightly coordinate the C-terminal part of the nascent peptide in the PTC of the ribosome. All of these interactions involve only the main-chain H-bond donor and acceptor atoms of the nascent polypeptide, and therefore are sequence-independent, which is critical for the ribosome's ability to translate virtually any sequences. While the existence of these H-bonds does not necessarily mean that they are required for efficient transpeptidation, there are several studies that support this hypothesis. For example, it has been demonstrated that the reactivity of a peptidyl-tRNA is modulated by the length of its nascent peptide chain: peptidyl-tRNAs with longer peptide chains react with puromycin (PMN) more rapidly than those with shorter ones^{47–49}. Based on these data, it has been hypothesized that the differences in the peptide bond formation rates with peptides of different lengths are due to tighter fixation of the longer nascent chains, and hence better positioning of the reactive groups in the PTC⁴⁸. Analysis of our structural data rationalizes this hypothesis. Indeed, while formyl-methionine forms only a single H-bond out of five possible peptide-stabilizing H-bonds, dipeptides and tripeptides can form three and five H-bonds, respectively, being more tightly restrained in the transpeptidation-competent conformation.

As evident from our structures, having more than three amino acid residues in a growing peptide chain does not provide any additional stabilization suggesting that the rate of transpeptidation should reach a plateau at a peptide length of -3 aa, a prediction that is in excellent agreement with the previous biochemical data⁴⁹.

The inability of proline residues to form some of these H-bonds, which could explain the apparent redundancy of interactions involving not just one but the three C-terminal residues of the growing peptide (positions 0, -1 and -2), is interesting. Despite a number of previous structural and functional studies $^{7,\bar{5}0,51}\!,$ there is no definitive answer to the fundamental question of why ribosome is unable to polymerize more than two consecutive prolines. In this case, ribosome stalling occurs due to the slow peptide bond formation between peptidyl-Pro-Pro-tRNA^{Pro} and Pro-tRNA^{Pro} located in the A site^{7,50}. Previous biochemical studies suggest that the poor reactivity of Pro-containing peptides stems from steric, rather than chemical, properties of this imino acid⁵². However, a mechanistic understanding of why peptidyl-Pro-Pro-tRNAs are especially inactive as P-site substrates is still lacking. In silico modelling reveals that the appearance of a single proline residue at any of the three C-terminal positions of the growing peptide chain results in the loss of some, but not all, of the peptide-restraining H-bonds (Extended Data Fig. 8), which provides incomplete yet sufficient stabilization of the conformation of the nucleophile acceptor, the carbonyl group, for the transpeptidation reaction

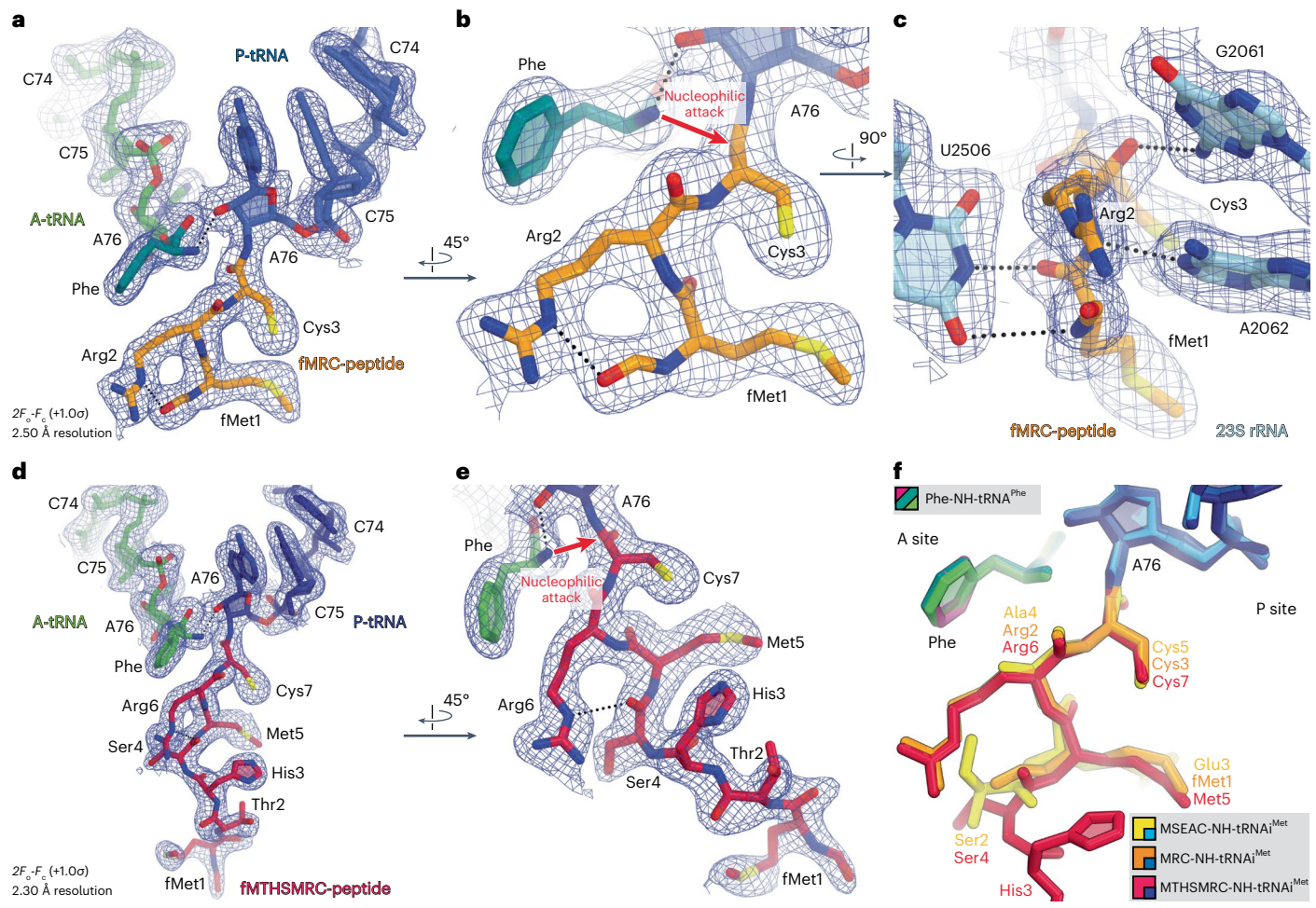


Fig. 5 | **Structure of the 70S ribosome in complex with fMRC- and fMTHSMRC-peptidyl-tRNAs. a-e**, Close-up views of the $2F_o-F_c$ electron difference Fourier map (blue mesh) of the ribosome complexes containing P-site fMRC-NH-tRNA_i^{Met} ($\mathbf{a}-\mathbf{c}$, blue with peptide highlighted in orange) or fMTHSMRC-NH-tRNA_i^{Met} ($\mathbf{d}-\mathbf{e}$, navy with peptide highlighted in crimson) and A-site Phe-NH-tRNA^{Phe} (green). Note that fMRC and fMTHSMRC peptides appear to be coordinated by the same network of H-bonds as the three C-terminal

residues of the fMSEAC-peptide shown in Fig. 3f. The views in panels \mathbf{a} , \mathbf{b} , \mathbf{c} and \mathbf{d} , \mathbf{e} represent different zoom levels and directions of the view as indicated by the arrows. \mathbf{f} , Superpositioning of the current three ribosome structures in complex with the full-length tRNAs carrying either fMSEAC (yellow), fMRC (orange) or fMTHSMRC (crimson) peptides in the P site. Note that the path of a peptide in the exit tunnel is not affected by the size of amino acid in the penultimate position.

to occur. This finding is corroborated by the biochemical data showing a significantly slower (~700-fold) rate of peptide bond formation with the C-terminal proline of the peptidyl-tRNA (ref. 48). However, the presence of two consecutive prolines in a growing polypeptide chain results in the loss of at least four out of five H-bonds (Extended Data Fig. 9a) that most certainly reduces the efficiency of the transpeptidation reaction because the poorly stabilized diprolyl-tRNA substrate with a wobbling carbonyl group is unlikely to be a good peptidyl donor during nucleophilic attack. What is more striking is that, unlike any other residue, modelling of the proline in the penultimate position of the growing peptide shows a substantial steric clash with the nucleotide A2062 of the 23S rRNA (Extended Data Figs. 8b and 9a), which is locked in place through a symmetric trans A-A Hoogsteen base pair with the residue A2503, suggesting that, during the passage of proline residues, the growing peptide must either deviate to the side or deflect A2062 to avoid this steric hindrance. Comparison of our model with the available structure of the ribosome-bound diprolyl-tRNA analogue confirmed our prediction, showing an alternate path of the Pro-Pro-containing peptide in the tunnel (Extended Data Fig. 9b)⁵³. Nevertheless, having two consecutive prolines in the peptide sequence does not result in a complete ribosome stalling⁷, most likely because the unstabilized wobbling peptidyl-tRNA could still randomly visit the productive conformation(s), and transpeptidation can still occur, albeit at a much slower rate . However, ribosome stalls completely when the next incoming amino acid is yet another proline residue . Most likely, this happens because the non-optimal position of the attacking A-site nucleophile is now combined with the poorly stabilized carbonyl group of the diprolyl-tRNA substrate in the P site. Thus, it becomes obvious that elongation factor P (EF-P), which is recruited to the ribosome every time two or more consecutive prolines need to be polymerized, provides stabilization of the otherwise wobbling diprolyl-tRNA substrate in the P site consistent with its previously proposed role in translation as an entropy-decreasing factor 7,50,51 .

Efficient protein synthesis requires tight coordination of A- and P-site substrates throughout all peptide bond formation events³⁶, including the first one. Analysis of our structure also provides insight into the possible role of formylation of initiator tRNA in bacteria. Superpositioning of the ribosome structure containing formylated initiator fMet-tRNA_i^{Met} in the P site with the structure of fMSEAC-peptidyl-tRNA reveals nearly identical positions of the carbon and oxygen atoms in the formyl group and those in the carbonyl group of the penultimate residue in the growing peptide chain (Extended Data Fig. 10). Similar to the carbonyl group, the formyl group is coordinated by the same nucleotide G2061 of the 23S rRNA, and thus provides additional

stabilization to the entire methionine residue attached to the P-site tRNA (Extended Data Fig. 10). In other words, during the first round of elongation, when only a single amino acid (and not yet a peptide) is present in the P site, the formyl group mimics a dipeptide and provides added coordination to the P-site substrate that otherwise would be available only to a dipeptidyl-tRNA. Consistent with our observation, the inability of non-formylated methionine residue to form a H-bond with the G2061 results in a fivefold decrease in the transpeptidation reaction rate⁵⁴.

Lack of the machinery for formylation of the initiator tRNA in eukaryotes could have been compensated in the course of evolution by acquiring a dedicated protein factor, such as eukaryotic initiation factor 5A (eIF-5A), that provides added stability to the first methionine residue, resulting in a more efficient transpeptidation. Although there is compelling evidence that both eukaryotic/archaeal eIF-5A and bacterial EF-P are needed primarily for the synthesis of polyproline stretches in proteins^{7,55,56}, and both carry functionally important hypermodified lysine residues that encroach upon the P-site substrate in the PTC 53,57, we cannot exclude the possibility that eIF-5A also contributes to formation of the first peptide bond as suggested by early reports^{58–60} in addition to its subsequently revealed general role in elongation and termination^{55,56}. These roles are not mutually exclusive, and it is conceivable that while diverging from a common ancestor, eIF-5A retained both of the original functions (facilitation of the first peptide bond formation and enhancement of transpeptidation, and nascent chain hydrolysis of problematic substrates during both elongation and termination, respectively), whereas EF-P retained only the second function, delegating the first to the initiator tRNA formylation machinery.

Curiously, the number of observed H-bonds established by the ribosome with the C-terminal part of the growing peptide is in striking contrast to the lack of any visible H-bonds with the peptide's N-terminal residues, suggesting that regardless of the length, only the C-terminal residues of the growing peptide need to be well coordinated for efficient protein synthesis and/or to prevent a rare spontaneous dissociation of the peptidyl-tRNA from the translating ribosome, an event known as drop-off⁶¹. Translation of particular sequences (especially in the presence of macrolide antibiotics) or polymerization of consecutive prolines and non-proteinogenic amino acids (such as β-, or N-methyl-amino acids), all of which are poor substrates for transpeptidation, promotes frequent peptidyl-tRNA drop-off events^{62,63}. Recently, EF-P was shown to efficiently prevent peptidyl-tRNA drop-offs not only on polyproline sequences but also on other problematic P-site substrates, pointing to its function in bacteria being more versatile than previously thought 63-65. Although the molecular mechanism of this phenomenon is yet to be elucidated, it is tempting to suggest that peptidyl-tRNA drop-off occurs when the C-terminal residues of a nascent chain are unable to establish most of the five H-bonds observed in our non-stalled RNCCs (Fig. 4), such as in the case with C-terminal Pro-Pro (Extended Data Fig. 9a) or D-Ala-D-Ala sequences⁶³. We hypothesize that the presence of multiple prolines, D-amino acids or other challenging nascent chain sequences results in the inability of the PTC to coordinate it well. This, in turn, leads to poor reactivity of the P-site substrate and, if a nascent chain is short, increases the chances of a peptidyl-tRNA drop-off.

While cysteine is one of the rarest amino acids in bacterial proteomes⁶⁶, and therefore unlikely to appear in the ultimate (C-terminal) position, many of the ribosome stalling peptides, such as ErmDL⁴⁵, preserve their full functionality even after the replacement of the C-terminal residue with cysteine and can be studied using our approach. The apparent limitation of our procedure is a requirement for the ultimate amino acid of the peptide chain to always be cysteine, dictated by the chemistry of the NCL reaction. However, the same limitation also exists with the widely used peptide/protein-only NCL, where multiple approaches have been utilized to overcome this limitation and extend the NCL reaction to other amino acids⁶⁷. For example, desulfurization of cysteine to alanine can be performed under mild conditions^{68,69} that

are unlikely to affect tRNA stability and, in principle, can be used to extend our methodology beyond Cys in the last position of the peptide.

Conclusions

We present here a simple, affordable and fast NCL-based method for the synthesis of peptidyl-tRNAs carrying nascent peptide chains of the desired sequences (except for the C-terminal Cys) that can be used in a wide range of structural and/or biochemical studies, especially those that are focused on understanding the role of nascent peptide sequence in the regulation of protein synthesis in response to various environmental cues, such as small molecules and antibiotics. By providing 2.3–2.5 Å resolution X-ray crystal structures of the RNCCs featuring hydrolysis-resistant aminoacyl-tRNA in the A site and peptidyl-tRNAs in the P site, we demonstrate that synthetic full-length peptidyl-tRNAs can efficiently be introduced into the ribosome in trans and yet represent a functionally significant pre-attack state of the PTC. The availability of such peptidyl-tRNAs opens avenues for structural studies of RNCCs under both stalling and non-stalling conditions in parallel, including rationalization of the context-specific mechanisms of action of many ribosome-targeting antibiotics such as those that target the PTC or the NPET. Moreover, detailed analysis of our structural data suggests a possible answer to the question of why ribosome is unable to polymerize more than two consecutive proline residues without the need for a dedicated facilitator (such as EF-P or eIF-5A). Furthermore, we provide important insights into the possible role of formylation of the initiator tRNA in the protein synthesis in bacteria. Finally, we propose a hypothesis that the C-terminal segments of all nascent peptides emerge in the same uniform β -strand conformation, which is yet to be verified experimentally as more structures of non-arrested RNCCs become available, especially now with the advent of this method for facile synthesis of full-length non-hydrolysable peptidyl-tRNAs by native chemical ligation.

Online content

Any methods, additional references, Nature Research reporting summaries, source data, extended data, supplementary information, acknowledgements, peer review information; details of author contributions and competing interests; and statements of data and code availability are available at https://doi.org/10.1038/s41557-022-01073-1.

References

- Bhushan, S. et al. α-Helical nascent polypeptide chains visualized within distinct regions of the ribosomal exit tunnel. Nat. Struct. Mol. Biol. 17, 313–317 (2010).
- Ito, K. & Chiba, S. Arrest peptides: cis-acting modulators of translation. Annu. Rev. Biochem. 82, 171–202 (2013).
- Vazquez-Laslop, N. & Mankin, A. S. How macrolide antibiotics work. Trends Biochem. Sci 43, 668–684 (2018).
- Wilson, D. N. Ribosome-targeting antibiotics and mechanisms of bacterial resistance. *Nat. Rev. Microbiol.* 12, 35–48 (2014).
- Lin, J., Zhou, D., Steitz, T. A., Polikanov, Y. S. & Gagnon, M. G. Ribosome-targeting antibiotics: modes of action, mechanisms of resistance, and implications for drug design. *Annu. Rev. Biochem.* 87, 451–478 (2018).
- Seip, B. & Innis, C. A. How widespread is metabolite sensing by ribosome-arresting nascent peptides? J. Mol. Biol. 428, 2217–2227 (2016).
- Doerfel, L. K. et al. EF-P is essential for rapid synthesis of proteins containing consecutive proline residues. Science 339, 85–88 (2013).
- Arenz, S. et al. A combined cryo-EM and molecular dynamics approach reveals the mechanism of ErmBL-mediated translation arrest. *Nat. Commun.* 7, 12026 (2016).
- Arenz, S. et al. Drug sensing by the ribosome induces translational arrest via active site perturbation. Mol. Cell 56, 446–452 (2014).

- Arenz, S. et al. Molecular basis for erythromycin-dependent ribosome stalling during translation of the ErmBL leader peptide. Nat. Commun. 5, 3501 (2014).
- Beckert, B. et al. Structural and mechanistic basis for translation inhibition by macrolide and ketolide antibiotics. *Nat. Commun.* 12, 4466 (2021).
- Herrero Del Valle, A. et al. Ornithine capture by a translating ribosome controls bacterial polyamine synthesis. *Nat. Microbiol.* 5, 554–561 (2020).
- Su, T. et al. The force-sensing peptide VemP employs extreme compaction and secondary structure formation to induce ribosomal stalling. *Elife* 6, e25642 (2017).
- Schaffitzel, C. & Ban, N. Generation of ribosome nascent chain complexes for structural and functional studies. *J. Struct. Biol.* 158, 463–471 (2007).
- Rutkowska, A. et al. Large-scale purification of ribosome-nascent chain complexes for biochemical and structural studies. FEBS Lett. 583, 2407–2413 (2009).
- Jha, S. S. & Komar, A. A. Using SecM arrest sequence as a tool to isolate ribosome bound polypeptides. J. Vis. Exp. 19, 4027 (2012).
- Cabrita, L. D. et al. A structural ensemble of a ribosomenascent chain complex during cotranslational protein folding. Nat. Struct. Mol. Biol. 23, 278–285 (2016).
- Cassaignau, A. M. et al. A strategy for co-translational folding studies of ribosome-bound nascent chain complexes using NMR spectroscopy. *Nat. Protoc.* 11, 1492–1507 (2016).
- Loveland, A. B., Demo, G. & Korostelev, A. A. Cryo-EM of elongating ribosome with EF-Tu*GTP elucidates tRNA proofreading. *Nature* 584, 640–645 (2020).
- Polikanov, Y. S., Steitz, T. A. & Innis, C. A. A proton wire to couple aminoacyl-tRNA accommodation and peptide-bond formation on the ribosome. *Nat. Struct. Mol. Biol.* 21, 787–793 (2014).
- Goto, Y. & Suga, H. Translation initiation with initiator tRNA charged with exotic peptides. J. Am. Chem. Soc. 131, 5040–5041 (2009).
- Fraser, T. H. & Rich, A. Synthesis and aminoacylation of 3'-amino-3'-deoxy transfer RNA and its activity in ribosomal protein synthesis. Proc. Natl Acad. Sci. USA 70, 2671–2675 (1973).
- Graber, D. et al. Reliable semi-synthesis of hydrolysis-resistant 3'-peptidyl-tRNA conjugates containing genuine tRNA modifications. *Nucleic Acids Res.* 38, 6796–6802 (2010).
- Dawson, P. E., Muir, T. W., Clark-Lewis, I. & Kent, S. B. Synthesis of proteins by native chemical ligation. Science 266, 776–779 (1994).
- Geiermann, A. S., Polacek, N. & Micura, R. Native chemical ligation of hydrolysis-resistant 3'-peptidyl-tRNA mimics. *J. Am. Chem. Soc.* 133, 19068–19071 (2011).
- Katoh, T. & Suga, H. Flexizyme-catalyzed synthesis of 3'-aminoacyl-NH-tRNAs. Nucleic Acids Res. 47, e54 (2019).
- 27. Gamper, H. & Hou, Y. M. tRNA 3'-amino-tailing for stable amino acid attachment. RNA **24**, 1878–1885 (2018).
- Svetlov, M. S. et al. Structure of Erm-modified 70S ribosome reveals the mechanism of macrolide resistance. *Nat. Chem. Biol.* 17, 412–420 (2021).
- Freist, W., Sternbach, H. & Cramer, F. Isoleucyl-tRNA synthetase from baker's yeast and from Escherichia coli MRE 600. Discrimination of 20 amino acids in aminoacylation of tRNA(Ile)-C-C-A(3'NH₂). Eur. J. Biochem. 169, 33–39 (1987).
- Schmitt, E., Blanquet, S. & Mechulam, Y. Crystallization and preliminary X-ray analysis of Escherichia coli methionyl-tRNAMet(f) formyltransferase complexed with formyl-methionyl-tRNAMet(f). Acta Crystallogr. D 55, 332–334 (1999).
- Vidales, F. J., Bernabeu, C. & Ballesta, J. P. Peptidyl transfer ribonucleic acid hydrolase activity of proteinase K. *Biochemistry* 18, 4155–4158 (1979).

- 32. Sothiselvam, S. et al. Macrolide antibiotics allosterically predispose the ribosome for translation arrest. *Proc. Natl Acad. Sci. USA* **111**. 9804–9809 (2014).
- Schmeing, T. M., Huang, K. S., Strobel, S. A. & Steitz, T. A. An induced-fit mechanism to promote peptide bond formation and exclude hydrolysis of peptidyl-tRNA. *Nature* 438, 520–524 (2005).
- Kuhlenkoetter, S., Wintermeyer, W. & Rodnina, M. V. Different substrate-dependent transition states in the active site of the ribosome. *Nature* 476, 351–354 (2011).
- Hiller, D. A., Singh, V., Zhong, M. & Strobel, S. A. A two-step chemical mechanism for ribosome-catalysed peptide bond formation. *Nature* 476, 236–239 (2011).
- Sievers, A., Beringer, M., Rodnina, M. V. & Wolfenden, R. The ribosome as an entropy trap. Proc. Natl Acad. Sci. USA 101, 7897–7901 (2004).
- Karimi, R., Pavlov, M. Y., Heurgue-Hamard, V., Buckingham, R. H. & Ehrenberg, M. Initiation factors IF1 and IF2 synergistically remove peptidyl-tRNAs with short polypeptides from the P-site of translating Escherichia coli ribosomes. *J. Mol. Biol.* 281, 241–252 (1998).
- Heurgue-Hamard, V. et al. Ribosome release factor RF4 and termination factor RF3 are involved in dissociation of peptidyl-tRNA from the ribosome. EMBO J. 17, 808–816 (1998).
- Youngman, E. M., Brunelle, J. L., Kochaniak, A. B. & Green, R.
 The active site of the ribosome is composed of two layers of conserved nucleotides with distinct roles in peptide bond formation and peptide release. Cell 117, 589–959 (2004).
- Sato, N. S., Hirabayashi, N., Agmon, I., Yonath, A. & Suzuki, T. Comprehensive genetic selection revealed essential bases in the peptidyl-transferase center. *Proc. Natl Acad. Sci. USA* 103, 15386–15391 (2006).
- 41. d'Aquino, A. E. et al. Mutational characterization and mapping of the 70S ribosome active site. *Nucleic Acids Res.* **48**, 2777–2789 (2020).
- 42. Koch, M., Willi, J., Pradere, U., Hall, J. & Polacek, N. Critical 23S rRNA interactions for macrolide-dependent ribosome stalling on the ErmCL nascent peptide chain. *Nucleic Acids Res.* **45**, 6717–6728 (2017).
- Vazquez-Laslop, N., Ramu, H., Klepacki, D., Kannan, K. & Mankin, A. S. The key function of a conserved and modified rRNA residue in the ribosomal response to the nascent peptide. *EMBO J.* 29, 3108–3117 (2010).
- 44. Syroegin, E. A. et al. Structural basis for the context-specific action of the classic peptidyl transferase inhibitor chloramphenicol. *Nat. Struct. Mol. Biol.* **29**, 152–161 (2022).
- Sothiselvam, S. et al. Binding of macrolide antibiotics leads to ribosomal selection against specific substrates based on their charge and size. Cell Rep. 16, 1789–1799 (2016).
- Lim, V. I. & Spirin, A. S. Stereochemical analysis of ribosomal transpeptidation. Conformation of nascent peptide. *J. Mol. Biol.* 188, 565–574 (1986).
- 47. Katunin, V. I., Muth, G. W., Strobel, S. A., Wintermeyer, W. & Rodnina, M. V. Important contribution to catalysis of peptide bond formation by a single ionizing group within the ribosome. *Mol. Cell* **10**, 339–346 (2002).
- 48. Wohlgemuth, I., Brenner, S., Beringer, M. & Rodnina, M. V. Modulation of the rate of peptidyl transfer on the ribosome by the nature of substrates. *J. Biol. Chem.* **283**, 32229–32235 (2008).
- 49. Panet, A., de Groot, N. & Lapidot, Y. Substrate specificity of *Escherichia coli* peptidyl-transferase. *Eur. J. Biochem.* **15**, 222–225 (1970).
- Woolstenhulme, C. J. et al. Nascent peptides that block protein synthesis in bacteria. Proc. Natl Acad. Sci. USA 110, E878–E887 (2013).

- Ude, S. et al. Translation elongation factor EF-P alleviates ribosome stalling at polyproline stretches. Science 339, 82–85 (2013).
- 52. Doerfel, L. K. et al. Entropic contribution of elongation factor P to proline positioning at the catalytic center of the ribosome. *J. Am. Chem.* Soc. **137**, 12997–13006 (2015).
- 53. Melnikov, S. et al. Molecular insights into protein synthesis with proline residues. *EMBO Rep.* **17**, 1776–1784 (2016).
- Bretscher, M. S. & Marcker, K. A. Polypeptidyl-sigma-ribonucleic acid and amino-acyl-sigma-ribonucleic acid binding sites on ribosomes. *Nature* 211, 380–384 (1966).
- Saini, P., Eyler, D. E., Green, R. & Dever, T. E. Hypusine-containing protein eIF5A promotes translation elongation. *Nature* 459, 118–121 (2009).
- Schuller, A. P., Wu, C. C., Dever, T. E., Buskirk, A. R. & Green, R. eIF5A functions globally in translation elongation and termination. *Mol. Cell* 66, 194–205 e195 (2017).
- Blaha, G., Stanley, R. E. & Steitz, T. A. Formation of the first peptide bond: the structure of EF-P bound to the 70S ribosome. *Science* 325, 966–970 (2009).
- Benne, R. & Hershey, J. W. The mechanism of action of protein synthesis initiation factors from rabbit reticulocytes. *J. Biol. Chem.* 253, 3078–3087 (1978).
- Kemper, W. M., Berry, K. W. & Merrick, W. C. Purification and properties of rabbit reticulocyte protein synthesis initiation factors M2Balpha and M2Bbeta. J. Biol. Chem. 251, 5551–5557 (1976).
- Schreier, M. H., Erni, B. & Staehelin, T. Initiation of mammalian protein synthesis. I. Purification and characterization of seven initiation factors. J. Mol. Biol. 116, 727–753 (1977).
- Menninger, J. R. Peptidyl transfer RNA dissociates during protein synthesis from ribosomes of Escherichia coli. J. Biol. Chem. 251, 3392–3398 (1976).
- 62. Fujino, T., Goto, Y., Suga, H. & Murakami, H. Reevaluation of the D-amino acid compatibility with the elongation event in translation. *J. Am. Chem. Soc.* **135**, 1830–1837 (2013).

- 63. Tajima, K., Katoh, T. & Suga, H. Drop-off-reinitiation triggered by EF-G-driven mistranslocation and its alleviation by EF-P. *Nucleic Acids Res.* **50**. 2736–2753 (2022).
- 64. Mohapatra, S., Choi, H., Ge, X., Sanyal, S. & Weisshaar, J. C. Spatial distribution and ribosome-binding dynamics of EF-P in live *Escherichia coli. mBio* **8** (2017).
- 65. Katoh, T., Iwane, Y. & Suga, H. Logical engineering of D-arm and T-stem of tRNA that enhances d-amino acid incorporation. *Nucleic Acids Res.* **45**, 12601–12610 (2017).
- Hormoz, S. Amino acid composition of proteins reduces deleterious impact of mutations. Sci Rep. 3, 2919 (2013).
- Kulkarni, S. S., Sayers, J., Premdjee, B. & Payne, R. J. Rapid and efficient protein synthesis through expansion of the native chemical ligation concept. *Nat. Rev. Chem.* 2, 0122 (2018).
- Wan, Q. & Danishefsky, S. J. Free-radical-based, specific desulfurization of cysteine: a powerful advance in the synthesis of polypeptides and glycopolypeptides. *Angew. Chem. Int. Ed. Engl.* 46, 9248–9252 (2007).
- Jin, K., Li, T., Chow, H. Y., Liu, H. & Li, X. P-B desulfurization: an enabling method for protein chemical synthesis and site-specific deuteration. *Angew. Chem. Int. Ed. Engl.* 56, 14607–14611 (2017).

Publisher's note Springer Nature remains neutral with regard to jurisdictional claims in published maps and institutional affiliations.

Springer Nature or its licensor holds exclusive rights to this article under a publishing agreement with the author(s) or other rightsholder(s); author self-archiving of the accepted manuscript version of this article is solely governed by the terms of such publishing agreement and applicable law.

© The Author(s), under exclusive licence to Springer Nature Limited 2022

Methods

Preparation of full-length tRNA_i^{Met} and tRNA^{Cys}

All reagents and chemicals were obtained from MilliporeSigma. Wild-type deacylated initiator tRNA_i^{Met} was overexpressed and purified from *E. coli* as described previously³⁰.

Cysteine-specific tRNA^{Cys} was purified essentially as described previously for glycine-specific tRNA^{Gly} with modifications⁷⁰. In brief, tRNA^{Cys} (GCA anticodon) encoding sequence from E. coli was cloned into the pBSTNAV plasmid vector using EcoRI and PstI restriction sites, resulting in the pBSTNAV-Cys vector for expression of tRNA^{Cys}. For large-scale preparation of tRNA^{Cys}, tRNA-expressing *E. coli* cells were grown overnight in LB media with 100 µg ml⁻¹ ampicillin. The cells were harvested and resuspended in buffer containing 1 mM Tris-HCl, pH 7.4, and 10 mM Mg(CH₂COO)₂, and treated with 0.5 vol of acidic phenol, pH 4.5. The aqueous phase was then precipitated by the addition of 2 vol of ethanol and NaCl to 500 mM final concentration. The resulting pellet was resuspended in 1 M NaCl, and the soluble fraction was precipitated with ethanol again. The pellet was resuspended in 200 mM Tris-HCl, pH 9.0, and the resulting solution of total tRNA was incubated for 2 h at 37 °C to promote deacylation of any remaining aa-tRNAs. Deacylated total tRNA was precipitated with ethanol, resuspended in buffer A (40 mM sodium phosphate buffer, pH 7.0), and subjected to anion exchange chromatography on an 8-ml MonoQ column (10/100 GL, GE Healthcare) using a 300-ml 0-100% linear gradient of buffer B (40 mM sodium phosphate buffer, pH 7.0, 1 M NaCl) for elution. Fractions containing the desired tRNA^{Cys} were identified by hybridization with the complementary oligonucleotide AGACG-GATTTGCAATCCGCTACATAACC, resulting in a gel-mobility shift⁷⁰, and by aminoacylation with cysteine which also results in a characteristic shift in the electrophoretic mobility (Extended Data Fig. 2b, lane 1 versus 2). All fractions containing tRNA^{Cys} were pooled together, precipitated with ethanol, resuspended in buffer C (20 mM NH₄CH₃COO, pH 5.5, 400 mM NaCl, 10 mM MgCl₂, 1 mM EDTA, 1% methanol), and subjected to reversed-phase chromatography on a 20-ml C5 column (C5-5, 250 × 10 mM, Discovery BIO Wide Pore, Supelco) using a 300-ml 0-60% linear gradient of buffer C supplemented with 40% methanol. Fractions containing tRNA^{Cys} were identified, pooled together and precipitated with ethanol as before. The final tRNA^{Cys} preparation was resuspended in 10 mM NH₄CH₃COO, pH 5.5, and assessed for purity and ability to accept cysteine using denaturing polyacrylamide gel electrophoresis (PAGE) and aminoacylation assay, respectively. The efficiency of aminoacylation of the final tRNA^{Cys} preparation was estimated to be greater than 90%.

Tailing of tRNA_i and tRNA^{Cys}

Tailing of tRNA_i^{Met} and tRNA^{Cys} (replacement of the 3′-terminal A76 nucleotide carrying the 3′-OH group with the one carrying 3′-NH₂) was performed as described previously with minor modifications²⁷. Briefly, deacylated tRNA_i^{Met} or tRNA^{Cys} (40 μ M) were incubated at 37 °C for 1 h in a buffer containing 100 mM glycine–NaOH, pH 9.0,1 mM dithiothreitol (DTT),1 mM pyrophosphate,1 mM 3′-NH₂-ATP (Axxora), and 10 μ M of the CCA-adding enzyme from *E. coli*. The reaction was terminated by the addition of EDTA to 20 mM, treated with 1:1 phenol–chloroform mixture (pH 8.0) and precipitated with ethanol. The resulting tRNA pellet was dissolved in 20–40 μ l of 10 mM NH₄CH₃COO, pH 5.5, and desalted via Sephadex G-25 (MilliporeSigma) spin columns (20–40 μ l of tRNA solution per 500 μ l of G-25 media).

Aminoacylation of tailed 3'-NH $_2$ -tRNA $_i^{Met}$ and 3'-NH $_2$ -tRNA Cys and native tRNA Cys

The following conditions were used for aminoacylation of tRNAs:

 For aminoacylation of the tailed 3'-NH₂-tRNA_i^{Met} with cysteine, 40 μM tRNA was incubated at 25 °C for 80 min in a buffer containing 100 mM HEPES–KOH, pH 8.2, 20 mM MgCl₂, 7.5 mM KCl₃

- $1\,\mathrm{mM}$ DTT, $10\,\mathrm{mM}$ ATP and $1\,\mathrm{mM}$ cysteine together with $1\,\mathrm{mg}$ ml $^{-1}$ methionine-specific aminoacyl-tRNA-synthetase (MetRS) from *E. coli*.
- For aminoacylation of the tailed 3'-NH₂-tRNA^{Cys} with cysteine, 40 μM tRNA was incubated at 37 °C for 16 h in a buffer containing 100 mM HEPES-KOH, pH 7.5, 20 mM MgCl₂, 30 mM KCl, 10 mM DTT, 10 mM ATP, 10 mM ascorbic acid, 1 mM EDTA and 10 mM cysteine together with 1 mg ml⁻¹ cysteine-specific aminoacyl-tRNA-synthetase (CysRS) from *E. coli*.
- For aminoacylation of the untailed (native) 3'-HO-tRNA^{Cys} with cysteine, 40 μM tRNA was incubated at 37 °C for 30 min in a buffer containing 40 mM HEPES-KOH, pH 7.5, 12.5 mM MgCl₂, 10 mM KCl, 10 mM DTT, 2.5 mM ATP and 2 mM cysteine together with 0.2 mg ml⁻¹ CysRS.

Aminoacylation reactions were terminated by the addition of EDTA to 30 mM concentration and then treated with phenol and precipitated with ethanol. The pellet was dissolved in a buffer containing 5 mM NaCH₃COO, 1 mM DTT, 0.1 mM EDTA to a final tRNA concentration of 20 μ g μ l⁻¹. Products were separated by acidic PAGE with 7 M urea.

Preparation of peptidyl-tRNAs

For native chemical ligation, dry thioester-activated peptides fMSEA-TBZ, fMR-TBZ or fMTHSMR-TBZ (98% purity) carrying a thio-benzyl group as the C-terminal modification (NovoPro Biosciences) were dissolved in a buffer containing 1 M HEPES-KOH, pH 7.4 and 6 M guanidine-HCl to obtain 50 mM final concentration. Next, 5 µl of the peptide solution was mixed with 15 µl of 400 mM 4-mercaptophenylacetic acid (MPAA) titrated to pH 7.0 with NaOH, and 20 µl of either non-hydrolysable amide-linked Cys-NH-tRNA_i Met or Cys-NH-tRNA^{Cys} or native ester-linked Cys-O-tRNA^{Cys}. Also, TCEP, pH 6.8, was added to the reaction mixture to 100 mM final concentration. The NCL reaction mixture was incubated for 16 hat room temperature. The NCL products were purified by HPLC on a 1.7-ml C4 reversed-phase column (Proteo 300, 100 × 4.6 mm; Higgins Analytical) using a 20-ml 0-60% linear gradient of 40% methanol in a buffer containing 20 mM NH₄CH₃COO, pH 5.5, 400 mM NaCl, 10 mM MgCl₂, 1 mM EDTA, 1% methanol and 10 mM β-mercaptoethanol. Before introduction into the C4 column, the NCL mixture was subjected to a buffer-exchange procedure using Amicon Ultra 10K centrifugal filter units (Millipore-Sigma). The fractions from the C4 column that contained the desired peptidyl-tRNAs were pooled, ethanol-precipitated and dissolved in a buffer containing 10 mM NH₄CH₃COO, pH 5.5, 5 mM DTT to 200 μ M final concentration. The aliquots were flash-frozen in liquid nitrogen and stored at -80 °C until further use in crystallization experiments.

Proteinase K treatment and gel electrophoresis of peptidyl-tRNA For proteinase K treatment, 1μ M of the C4-purified fMSEAC-NH-tRNA_i was incubated with 0.4 mg ml⁻¹ proteinase K (MilliporeSigma) in a

buffer containing 10 mM Tris-acetate, pH 8.0, 10 mM Mg(CH $_3$ COO) $_2$ and 40 mM NH $_4$ CH $_3$ COO for 1 h at 25 °C. The reaction was terminated by the addition of 2 vol of formamide electrophoresis buffer containing 10% β -mercaptoethanol and heating for 2 min at 95 °C. For separation of the NCL products, we used denaturing 8% (19:1) PAGE in the presence of 7 M urea (20-cm-long and 0.4-mm-thick gels). Gels were stained with ethidium bromide and visualized with Alpha Imager (Alpha Innotek).

X-ray crystallographic structure determination

Wild-type 70S ribosomes from *T. thermophilus* (strain HB8) were prepared as described previously^{20,71-73}. Synthetic mRNA with the sequence 5'-<u>GGC-AAG-GAG-GUA-AAA</u>-AUG-UUC-UAA-3' containing the Shine–Dalgarno sequence (underlined) followed by methionine (AUG) and phenylalanine (UUC) codons was obtained from Integrated DNA Technologies. Non-hydrolysable aminoacylated Phe-NH-tRNA^{Phe} was prepared as described previously²⁸ using the

optimized 3'-NH2-tailing and aminoacylation procedures described above²⁷. Complexes of the wild-type *T. thermophilus* 70S ribosomes with mRNA and hydrolysis-resistant aminoacyl (A-site Phe-NH-tRNA Phe) and peptidyl (P-site fMSEAC-NH-tRNA_i^{Met}, or fMRC-NH-tRNA_i^{Met}, or fMTHSMRC-NH-tRNA_i^{Met}) tRNAs were formed as described previously for deacylated⁷³ or aminoacylated tRNAs^{20,28}. Functionally relevant binding of aminoacyl- and peptidyl-tRNAs to the A and P sites, respectively, was achieved without the use of auxiliary initiation or elongation factors. Collection and processing of the X-ray diffraction data, model building and structure refinement were performed as described in our previous publications^{20,28,44,72,73}. The statistics of data collection and refinement are compiled in Table 1. All figures showing atomic models were rendered using PyMOL Molecular Graphics System software (v. 1.8.6, Schrödinger, www.pymol.org), Extended Data Fig. 5 showing Ramachandran plots was rendered using UCSF ChimeraX software (v. 1.3)74.

Reporting summary

Further information on research design is available in the Nature Research Reporting Summary linked to this article.

Data Availability

Coordinates and structure factors were deposited in the RCSB Protein Data Bank with the following accession codes: 8CVJ for the *T. thermophilus* 70S ribosome in complex with mRNA, aminoacylated A-site Phe-NH-tRNA^{Phe}, peptidyl P-site fMSEAC-NH-tRNA_i^{Met} and deacylated E-site tRNA^{Phe}; 8CVK for the *T. thermophilus* 70S ribosome in complex with mRNA, aminoacylated A-site Phe-NH-tRNA^{Phe}, peptidyl P-site fMRC-NH-tRNA_i^{Met} and deacylated E-site tRNA^{Phe}; 8CVL for the *T. thermophilus* 70S ribosome in complex with mRNA, aminoacylated A-site Phe-NH-tRNA^{Phe}, peptidyl P-site fMTHSMRC-NH-tRNA_i^{Met} and deacylated E-site tRNA^{Phe}, peptidyl P-site fMTHSMRC-NH-tRNA_i^{Met} and deacylated E-site tRNA^{Phe}. All previously published structures that were used in this work for model building and structural comparisons were retrieved from the RCSB Protein Data Bank: PDB entries 6XHW, 6WDD, 6TC3, 5NWY and 5DGV. Source data are provided with this paper.

References

- Degut, C., Monod, A., Brachet, F., Crepin, T. & Tisne, C. In vitro/ in vivo production of tRNA for X-ray studies. *Methods Mol. Biol.* 1320, 37–57 (2016).
- Selmer, M. et al. Structure of the 70S ribosome complexed with mRNA and tRNA. Science 313, 1935–1942 (2006).
- Polikanov, Y. S., Blaha, G. M. & Steitz, T. A. How hibernation factors RMF, HPF, and YfiA turn off protein synthesis. Science 336, 915–918 (2012).
- 73. Polikanov, Y. S., Melnikov, S. V., Soll, D. & Steitz, T. A. Structural insights into the role of rRNA modifications in protein synthesis and ribosome assembly. *Nat. Struct. Mol. Biol.* **22**, 342–344 (2015).
- Pettersen, E. F. et al. UCSF ChimeraX: structure visualization for researchers, educators, and developers. Protein Sci. 30, 70–82 (2021).
- Vimberg, V., Xiong, L., Bailey, M., Tenson, T. & Mankin, A. Peptide-mediated macrolide resistance reveals possible specific interactions in the nascent peptide exit tunnel. *Mol. Microbiol.* 54, 376–385 (2004).

- Marks, J. et al. Context-specific inhibition of translation by ribosomal antibiotics targeting the peptidyl transferase center. Proc. Natl Acad. Sci. USA 113, 12150–12155 (2016).
- Florin, T. et al. An antimicrobial peptide that inhibits translation by trapping release factors on the ribosome. *Nat. Struct. Mol. Biol.* 24, 752–757 (2017).

Acknowledgements

We thank R. Micura, A. Mankin, N. Vazquez-Laslop and M. Svetlov for critical reading of the manuscript and valuable suggestions. We thank I. Kamyshko for providing expertise in reagent and material sourcing. We thank the staff at NE-CAT beamlines 24ID-C and 24ID-E for help with data collection and freezing of the crystals, especially M. Capel, F. Murphy, S. Baneriee, I. Kourinov, D. Neau, J. Schuermann, N. Sukumar, A. Lynch, J. Withrow, K. Perry, A. Kaya and C. Salbego. This work is based upon research conducted at the Northeastern Collaborative Access Team beamlines, which are funded by the National Institute of General Medical Sciences from the National Institutes of Health (P30-GM124165 to NE-CAT). The Eiger 16M detector on the 24-ID-E beamline is funded by an NIH-ORIP HEI grant (S10-OD021527 to NE-CAT). This research used resources of the Advanced Photon Source, a US Department of Energy (DOE) Office of Science User Facility operated for the DOE Office of Science by Argonne National Laboratory under contract number DE-ACO2-06CH11357. This work was supported by the National Institutes of Health (RO1-GM132302 and R21-Al163466 to Y.S.P.), the National Science Foundation (MCB-1907273 to Y.S.P.) and Illinois State start-up funds (to Y.S.P.). The funders had no role in study design, data collection and analysis, decision to publish or preparation of the manuscript.

Author contributions

E.A.S. with help from E.V.A. developed the NCL-based method for the synthesis of non-hydrolysable full-length peptidyl-tRNAs. E.A.S., E.V.A. and Y.S.P. designed and performed X-ray crystallography experiments. Y.S.P. supervised the experiments. All authors interpreted the results. E.A.S., E.V.A. and Y.S.P. wrote the manuscript.

Competing interests

The authors declare no competing interests.

Additional information

Extended data is available for this paper at https://doi.org/10.1038/s41557-022-01073-1.

Supplementary information The online version contains supplementary material available at https://doi.org/10.1038/s41557-022-01073-1.

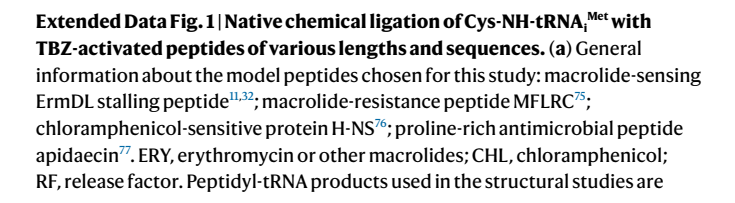
Correspondence and requests for materials should be addressed to Yury S. Polikanov.

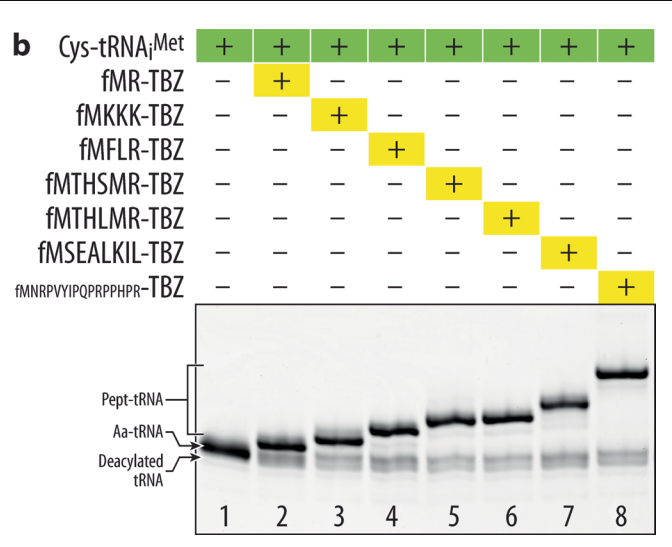
Peer review information *Nature Chemistry* thanks the anonymous reviewer(s) for their contribution to the peer review of this work.

Reprints and permissions information is available at www.nature.com/reprints.

a

Source Gene Product	Original Peptide Sequence	Translation Arrest in the Presence of	Synthetic TBZ-activated Peptide for NCL	Final peptidyl-tRNA Product
ErmDL	MRL	ERY & R/K in the A site	fMR-TBZ	fMRC-tRNA
-	MKKK	No Stalling	fMKKK-TBZ	fMKKKC-tRNA
-	MFLRC	Unknown	fMFLR-TBZ	fMFLRC-tRNA
ErmDL	MTHSMRL	ERY & R/K in the A site	fMTHSMR-TBZ	fMTHSMRC-tRNA
ErmDL	MTHLMRL	No Stalling	fMTHLMR-TBZ	fMTHLMRC-tRNA
H-NS	MSEAL	CHL & not G in the A site	fMSEA-TBZ	fMSEAC-tRNA
H-NS	MSEALKILN	CHL & not G in the A site	fMSEALKIL-TBZ	fMSEALKILC-tRNA
Apidaecin	MNRPVYIPQPRPPHPRL	RF and deac-tRNA	fmnrpvyipqprpphpr-tbz	fMNRPVYIPQPRPPHPRC-tRNA

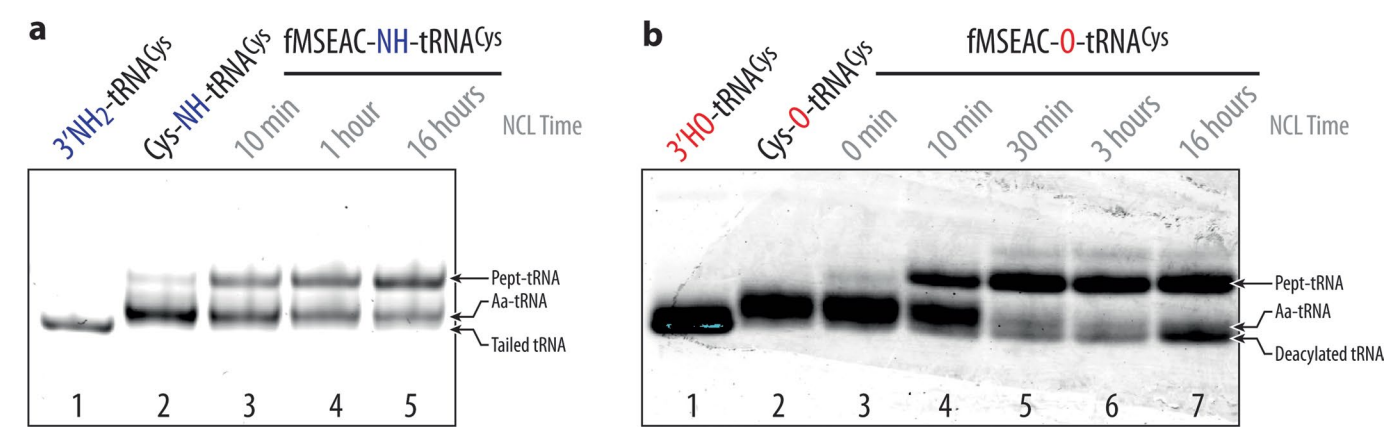




highlighted in grey. (**b**) Electrophoretic separation of crude NCL reaction mixtures. Indicated TBZ-activated peptides and Cys-NH-tRNA_i^{Met} were used as N-and C-terminal reactants, respectively. Electrophoresis was performed in 20-cm long 8% PAAG with 7 M urea and stained with ethidium bromide. Note the slower mobility of tRNA after the NCL that is also proportional to the ligated peptide length (lanes $2-8\,\nu s$. 1).

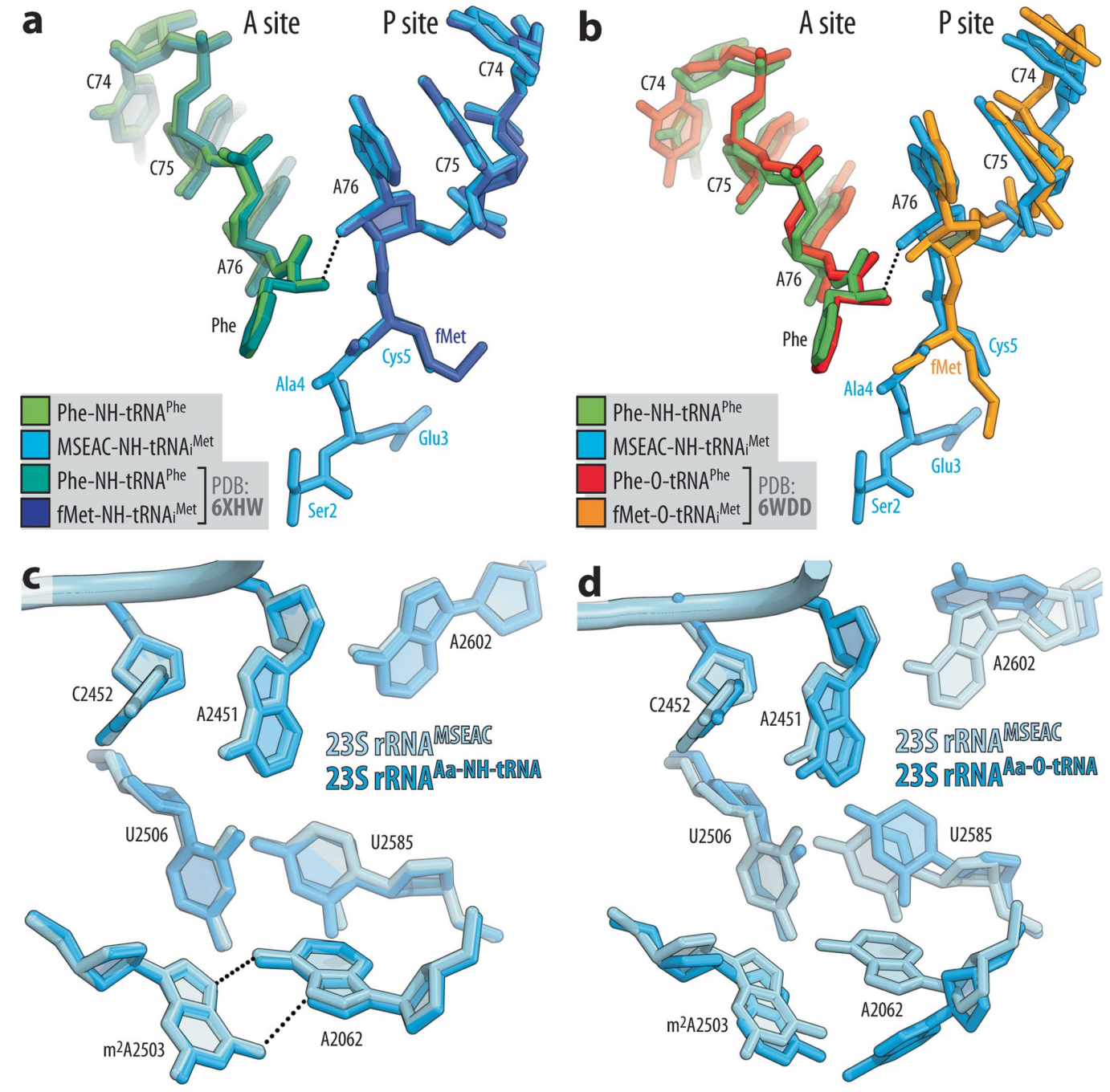
Pept-tRNA

Aa-tRNA



Extended Data Fig. 2 | Native chemical ligation of non-hydrolyzable or native Cys-tRNA^{Cys} with TBZ-activated fMSEA-peptide. (a, b) Electrophoretic separations of deacylated, aminoacyl- and peptidyl-tRNA^{Cys} before and after NCL reactions. Amino-tailed 3'-NH₂-tRNA^{Cys} (a, lane 1) or native 3'-HO-tRNA^{Cys} (b, lane

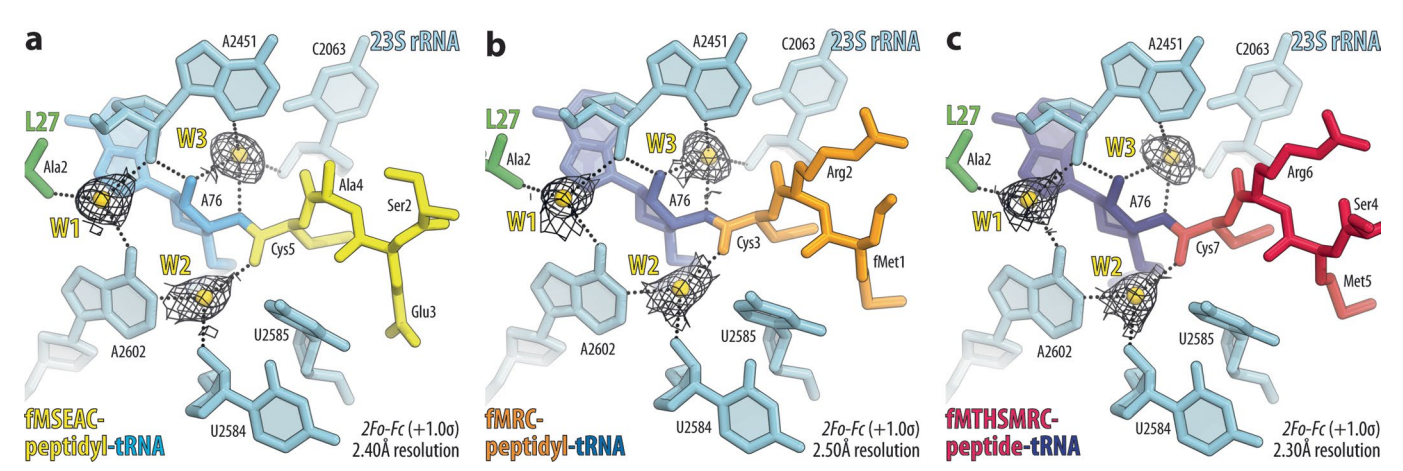
 $1)\,were\,first\,aminoacylated\,using\,cysteine\text{-}specific\,aminoacyl\text{-}tRNA\text{-}synthetase}$ (lanes 2) and then ligated with activated fMSEA-TBZ peptide for various times (lanes 3–5 in ${f a}$ and 3–7 in ${f b}$) to yield either non-hydrolyzable fMSEAC-NH-tRNA cys (a) or native ester-linked fMSEAC-O-tRNA^{Cys} (b) peptidyl-tRNAs.



Extended Data Fig. 3 | Comparison of the structures of fMSEAC-peptidyl-tRNA with aminoacylated full-length tRNAs. (a, b)

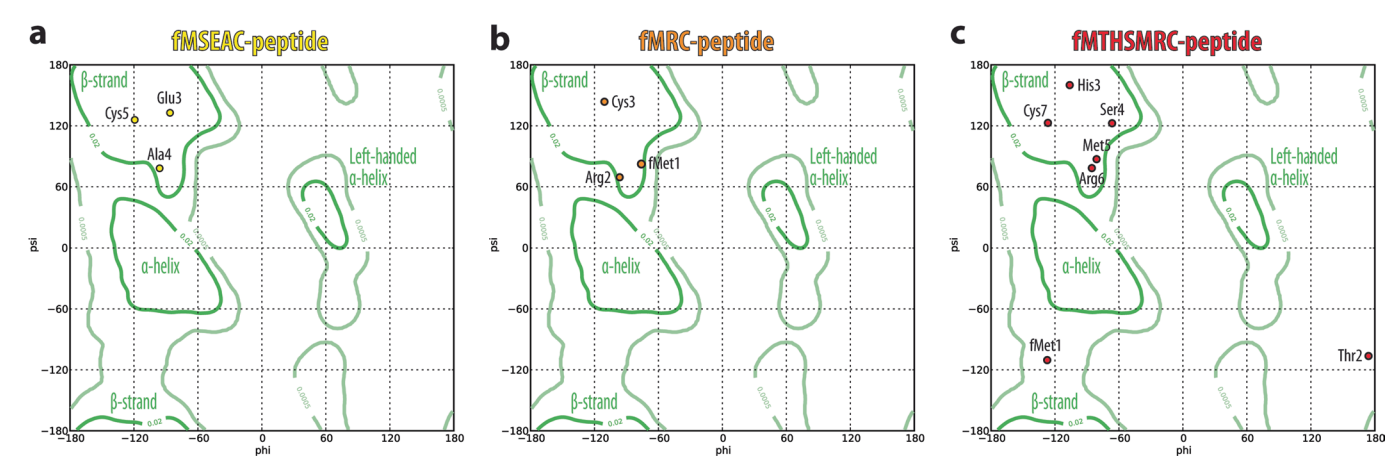
Superpositioning of our 70S ribosome structure carrying Phe-NH-tRNA $^{\rm Phe}$ (green) and fMSEAC-NH-tRNA, $^{\rm Met}$ (blue) in the A and P sites, respectively, with the previously reported structures of ribosome-bound full-length aminoacyl-tRNAs featuring either non-hydrolyzable amide linkages (a, PDB entry 6XHW 28) or native ester bonds (b, PDB entry 6WDD 19) between the amino acid moieties and

the ribose of nucleotide A76 of A- and P-site tRNAs. All structures were aligned based on domain V of the 23S rRNA. (\mathbf{c} , \mathbf{d}) Comparisons of the positions of key 23S rRNA nucleotides around the PTC in the same structures. Note that there are no significant differences in the positions of A- or P-site substrates or the PTC nucleotides indicating that the amide-linked aminoacyl and peptidyl-tRNAs represent functionally meaningful analogs of native ester-linked tRNAs.



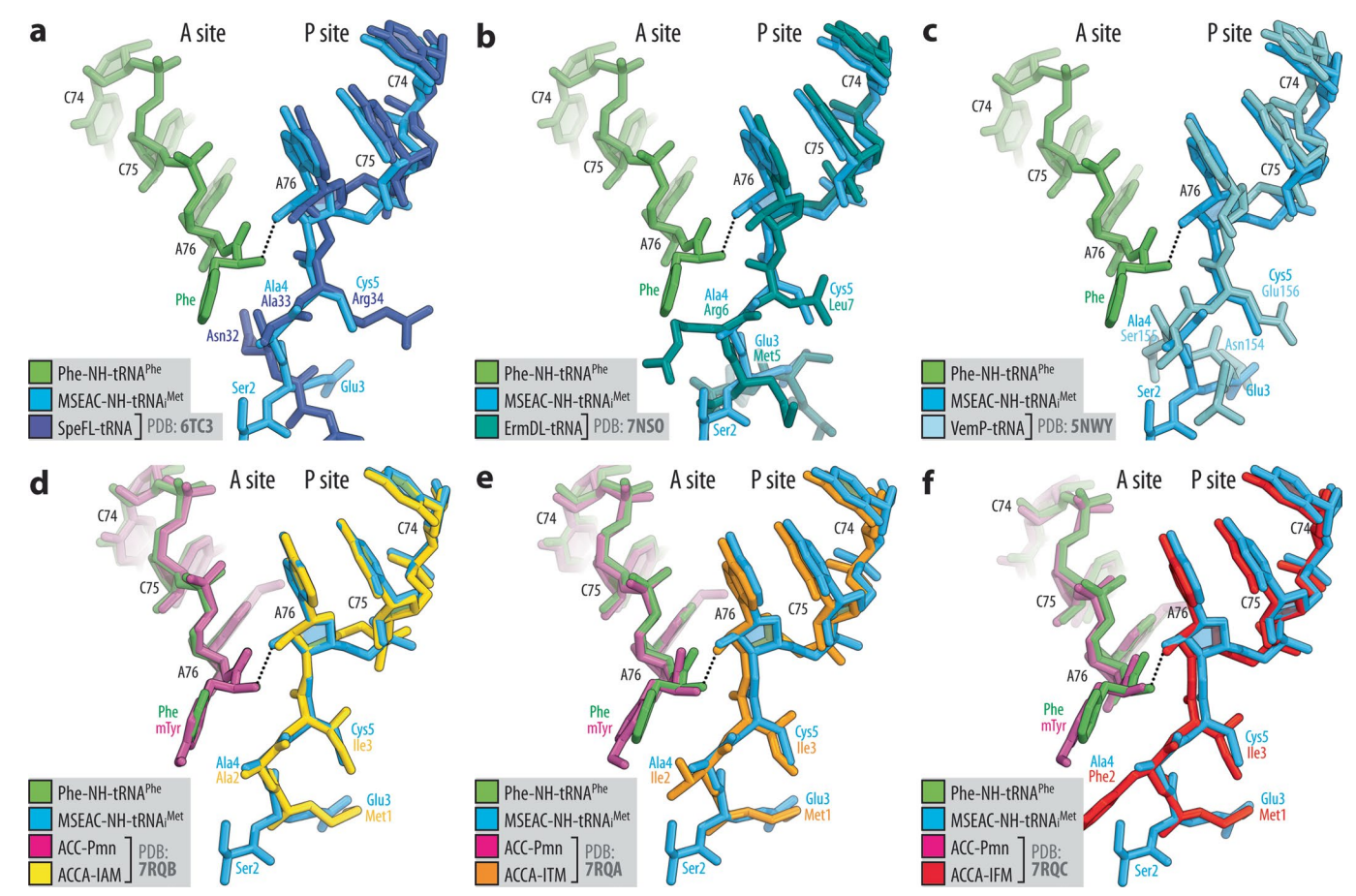
Extended Data Fig. 4 | Tightly coordinated water molecules in the pre-attack state of the peptidyl transferase center. (a-c) Close-up views of the $2F_o$ - F_c electron difference Fourier map (black mesh) for water molecules W1, W2, and W3 (yellow; nomenclature from 20) in the pre-peptidyl-transfer

complex structures featuring Phe-NH-tRNA $^{\rm Phe}$ in the A site (omitted for clarity) and fMSEAC-NH-tRNA $^{\rm Met}_i$ (a, yellow), fMRC-NH-tRNA $^{\rm Met}_i$ (b, orange), or fMTHSMRC-NH-tRNA $^{\rm Met}_i$ (c, crimson) in the P site. H-bonds are shown by black dotted lines.



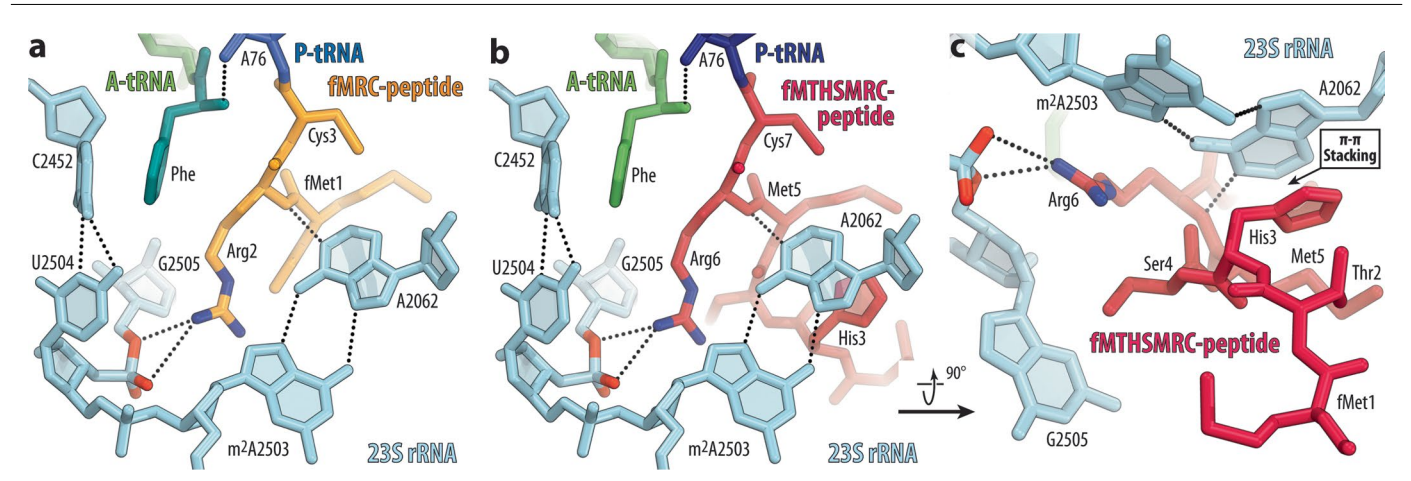
Extended Data Fig. 5 | Ramachandran plots for the peptide moieties of the ribosome-bound peptidyl-tRNAs. (a-c) Diagrams of the phi vs. psi angles for amino acid residues in fMSEAC-NH-tRNA_i $^{\text{Met}}$ (a, yellow), fMRC-NH-tRNA_i $^{\text{Met}}$ (b, orange), or fMTHSMRC-NH-tRNA_i $^{\text{Met}}$ (c, crimson) in the P site. Favored regions

are shown in green; allowed regions are light green. Due to the absence of fMet1 residue in the structure of fMSEAC-peptidyl-tRNA, phi angle for the subsequent Ser2 residue cannot be determined.



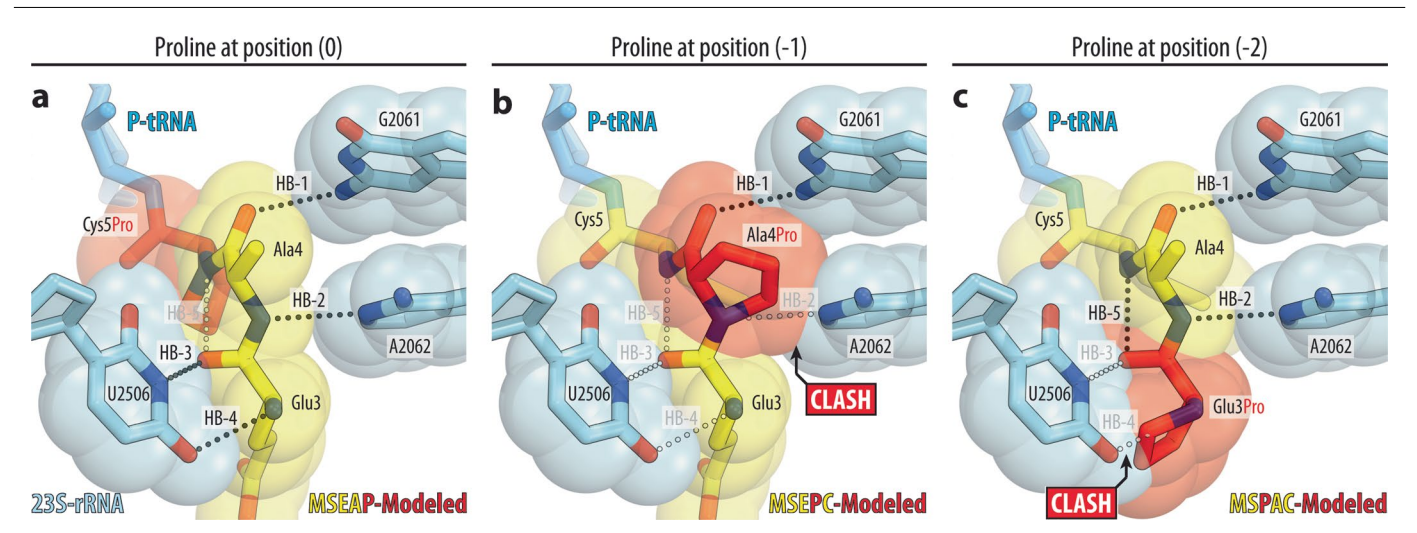
Extended Data Fig. 6 | Comparison of the structures of fMSEAC-peptidyl-tRNA with the structures of other ribosome-bound peptidyl-tRNAs. Superpositioning of the 70S ribosome structure containing A-site Phe-NH-tRNA Phe (green) and P-site fMSEAC-NH-tRNA; Met (blue) with the previously reported structures of stalled RNCCs carrying full-length peptidyl-tRNAs (a-c) or non-stalled RNCCs carrying short non-hydrolyzable tripeptidyl-tRNA analogs (d-f). Individual panels show comparisons of the

fMSEAC-tripeptidyl-tRNA with the following peptides: (a) SpeFL (dark blue, PDB entry 6TC3 12); (b) ErmDL (teal, PDB entry 7NSO 11), (c) VemP (cyan, PDB entry 5NWY 13); (d) MAI-tripeptide (yellow, PDB entry 7RQB 44); (e) MTI-tripeptide (orange, PDB entry 7RQA 44), (f) MFI-tripeptide (red, PDB entry 7RQC 44). All structures were aligned based on domain V of the 23S rRNA. Note that the overall path of the fMSEAC-peptide in our structure is similar to the trajectories of the other peptides in the NPET.



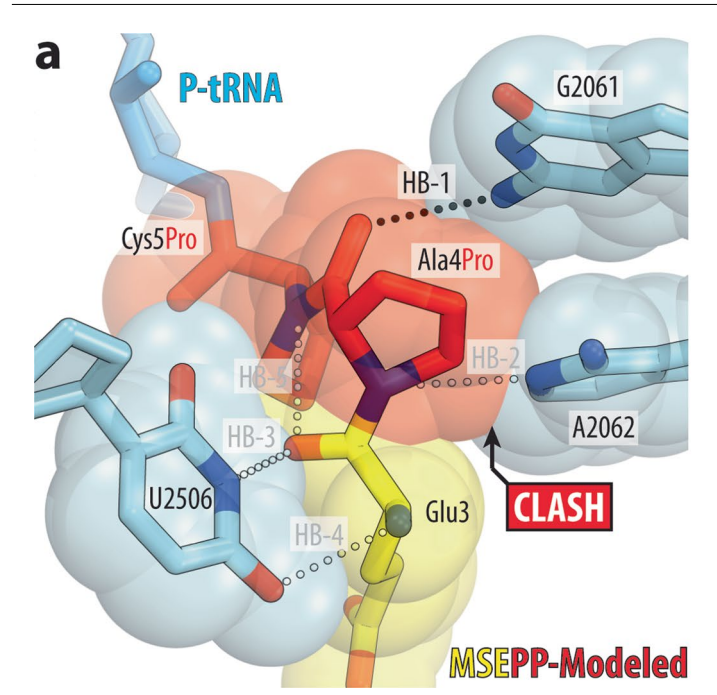
Extended Data Fig. 7 | Additional interactions of the side chains of fMRC- and fMTHSMRC-peptidyl-tRNAs with the ribosome. (a, b) Close-up views of the electrostatic interactions between the side chain of the penultimate Arg residue of the P-site fMRC-NH-tRNA $_i^{\text{Met}}$ (a, blue with peptide highlighted in orange) or

fMTHSMRC-NH-tRNA $_{\rm i}^{\rm Met}$ (b, navy with peptide highlighted in crimson) and the phosphate of nucleotide G2505 of the 23S rRNA. H-bonds are shown by black dotted lines. (c) Stacking interactions between the aromatic side chain of His3 of fMTHSMRC-peptidyl-tRNA and A2062 nucleobase of the 23S rRNA.

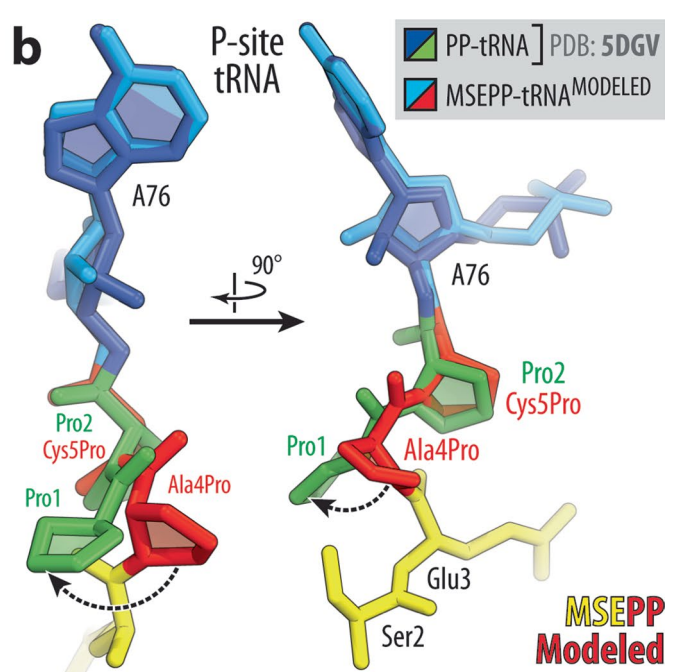


Extended Data Fig. 8 | **Proline residues in the nascent peptide are unable to form stabilizing H-bonds in the NPET. (a-c)** *In silico* modeling of proline residues at ultimate (a, CysSPro), penultimate (b, Ala4Pro), or pen-penultimate (c, Glu3Pro) positions of the fMSEAC-peptide chain. Note that besides its inability

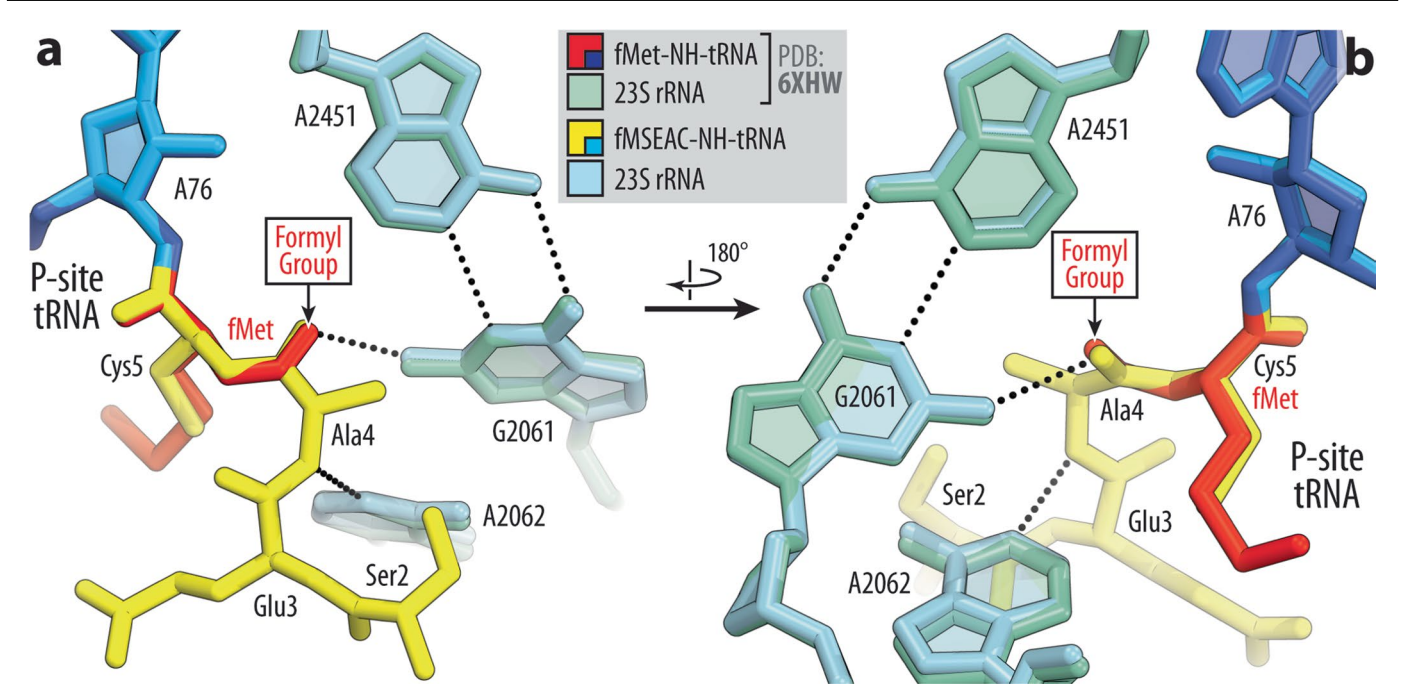
to form most of the peptide-stabilizing H-bonds, proline in the penultimate and pen-penultimate positions clashes with nucleotides A2062 and U2506 of the 23S rRNA, respectively. Geometrically possible and impossible H-bonds are shown by black and white dotted lines, respectively.



Extended Data Fig. 9 | **Proline residues alter the path of the nascent peptide in the NPET. (a)** *In silico* modeling of the two consecutive proline residues at ultimate (CysSPro) and penultimate (Ala4Pro) positions of the fMSEAC-peptide chain. Note that, due to the side chains, the diproline-containing peptide cannot adopt a conformation possible for other peptides in the NPET and must re-orient. **(b)** Comparison of the previous structure of ribosome-bound short



diprolyl-tRNA analog (green, PDB entry 5DGV 53) with the in silico-modeled diprolyl-containing tRNA based on the structure of fMSEAC-peptidyl-tRNA (red). Note that in order to avoid a steric clash with the A2062, the diprolyl moiety of the nascent peptide deviates to the side (black dashed arrows) and, thus, has an alternative path in the NPET.



Extended Data Fig. 10 | Formylation of the first methionine residue provides additional stability to the initiator tRNA substrate in the P site. Superpositioning of the previous structure of ribosome-bound initiator fMet-NH-tRNA $_i^{\text{Met}}$ (navy with the fMet moiety in red, PDB entry 6XHW 28) with the new structure of fMSEAC-peptidyl-tRNA (blue with the peptide moiety

highlighted in yellow) viewed from two opposite sides (a,b). H-bonds are shown by black dotted lines. Note that the positions of carbon and oxygen atoms in the formyl group and those in the carbonyl group of the penultimate residue in the nascent peptide chain are nearly identical, ensuring formation of the same H-bond with the exocyclic amino group of the G2061 residue.

nature portfolio

Corresponding author(s):	Yury Polikanov
Last updated by author(s):	06/17/2022

Reporting Summary

Nature Portfolio wishes to improve the reproducibility of the work that we publish. This form provides structure for consistency and transparency in reporting. For further information on Nature Portfolio policies, see our Editorial Policies and the Editorial Policy Checklist.

<u> </u>						
∨ †	٠.	t١	C	ŀι	\sim	c

FOI 6	an statistical analyses, commit that the following items are present in the figure legend, table legend, main text, or Methods section.
n/a	Confirmed
\boxtimes	The exact sample size (n) for each experimental group/condition, given as a discrete number and unit of measurement
\boxtimes	A statement on whether measurements were taken from distinct samples or whether the same sample was measured repeatedly
\boxtimes	The statistical test(s) used AND whether they are one- or two-sided Only common tests should be described solely by name; describe more complex techniques in the Methods section.
\boxtimes	A description of all covariates tested
\boxtimes	A description of any assumptions or corrections, such as tests of normality and adjustment for multiple comparisons
\boxtimes	A full description of the statistical parameters including central tendency (e.g. means) or other basic estimates (e.g. regression coefficient) AND variation (e.g. standard deviation) or associated estimates of uncertainty (e.g. confidence intervals)
\boxtimes	For null hypothesis testing, the test statistic (e.g. <i>F</i> , <i>t</i> , <i>r</i>) with confidence intervals, effect sizes, degrees of freedom and <i>P</i> value noted <i>Give P values as exact values whenever suitable.</i>
\boxtimes	For Bayesian analysis, information on the choice of priors and Markov chain Monte Carlo settings
\boxtimes	For hierarchical and complex designs, identification of the appropriate level for tests and full reporting of outcomes
\boxtimes	Estimates of effect sizes (e.g. Cohen's <i>d</i> , Pearson's <i>r</i>), indicating how they were calculated
	Our web collection on statistics for biologists contains articles on many of the points above

Software and code

Policy information about availability of computer code

Data collection

X-ray diffraction data was collected at beamlines 24ID-C and 24ID-E at the Advanced Photon Source (Argonne National Laboratory) using NE-CAT Remote Access software v6.2.0.

Data analysis

Raw X-ray crystallographic data were integrated and scaled using XDS software (Feb 5, 2021). Molecular replacement was performed using PHASER from the CCP4 program suite (version 7.0). All structures were refined using PHENIX software (version 1.17). Structural models were built in Coot (version 0.8.2). All figures showing atomic models were generated using PyMol software (version 1.8). Ramachandran plots was rendered using UCSF ChimeraX software (version 1.3).

For manuscripts utilizing custom algorithms or software that are central to the research but not yet described in published literature, software must be made available to editors and reviewers. We strongly encourage code deposition in a community repository (e.g., GitHub). See the Nature Portfolio guidelines for submitting code & software for further information.

Data

Policy information about availability of data

All manuscripts must include a data availability statement. This statement should provide the following information, where applicable:

- Accession codes, unique identifiers, or web links for publicly available datasets
- A description of any restrictions on data availability
- For clinical datasets or third party data, please ensure that the statement adheres to our policy

Coordinates and structure factors were deposited in the RCSB Protein Data Bank with accession codes:

• 8CVJ for the T. thermophilus 70S ribosome in complex with mRNA, aminoacylated A-site Phe-NH-tRNAPhe, peptidyl P-site fMSEAC-NH-tRNAiMet, and deacylated E-site tRNAPhe;

 8CVK for the 	e T. thermophilus	70S ribosome i	n complex with n	nRNA, amino	pacylated A-si	te Phe-NH-tRNAPhe	e, peptidyl P-s	ite fMRC-NH-t	tRNAiMet, a	and deacy	lated E-
site tRNAPhe;											

• 8CVL for the T. thermophilus 70S ribosome in complex with mRNA, aminoacylated A-site Phe-NH-tRNAPhe, peptidyl P-site fMTHSMRC-NH-tRNAiMet, and deacylated E-site tRNAPhe.

				٠.				
FIPI	\cap	I-sr)ec	ITIC	re	ററ	rtir	ŊØ
	. ~	'	,	1110		\sim		מי

Please select the o	ne below that is the best fit for your research. If you are not sure, read the appropriate sections before making your selection.
X Life sciences	Behavioural & social sciences Ecological, evolutionary & environmental sciences
For a reference copy of t	the document with all sections, see nature.com/documents/nr-reporting-summary-flat.pdf
Life scier	nces study design
All studies must dis	close on these points even when the disclosure is negative.
Sample size	Not Applicable
Data exclusions	Not Applicable
Replication	Not Applicable
Randomization	Not Applicable
Blinding	Not Applicable

Reporting for specific materials, systems and methods

We require information from authors about some types of materials, experimental systems and methods used in many studies. Here, indicate whether each material, system or method listed is relevant to your study. If you are not sure if a list item applies to your research, read the appropriate section before selecting a response.

Materials & experimental systems	Methods			
n/a Involved in the study	n/a Involved in the study			
Antibodies	ChIP-seq			
Eukaryotic cell lines	⊠ Flow cytometry			
Palaeontology and archaeology	MRI-based neuroimaging			
Animals and other organisms	·			
Human research participants				
Clinical data				
Dual use research of concern				